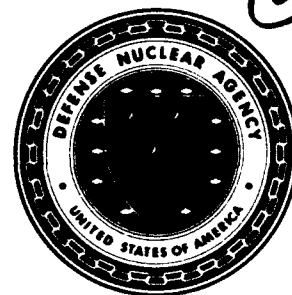




AD-A275 235



**Defense Nuclear Agency
Alexandria, VA 22310-3398**



DNA-TR-93-50

Modeling the Total Dose Radiation Effects of $\text{Hg}_{1-x}\text{Cd}_x\text{Te}$ Photodiodes Using Numerical Device Simulators

**James C. Petrosky, et al.
Rensselaer Polytechnic Institute
P.O. Box 965
Troy, NY 12181**

January 1994

**DTIC
ELECTE
FEB 02 1994
S B D**

Technical Report

CONTRACT No. DNA MIPR-92-501

**Approved for public release;
distribution is unlimited.**

94-03118

94 1 31 174

Destroy this report when it is no longer needed. Do not return to sender.

PLEASE NOTIFY THE DEFENSE NUCLEAR AGENCY,
ATTN: CSTI, 6801 TELEGRAPH ROAD, ALEXANDRIA, VA
22310-3398, IF YOUR ADDRESS IS INCORRECT, IF YOU
WISH IT DELETED FROM THE DISTRIBUTION LIST, OR
IF THE ADDRESSEE IS NO LONGER EMPLOYED BY YOUR
ORGANIZATION.



DISTRIBUTION LIST UPDATE

This mailer is provided to enable DNA to maintain current distribution lists for reports. (We would appreciate your providing the requested information.)

- ☐ Add the individual listed to your distribution list.
- ☐ Delete the cited organization/individual.
- ☐ Change of address.

NOTE:

Please return the mailing label from the document so that any additions, changes, corrections or deletions can be made easily.

NAME: _____

ORGANIZATION: _____

OLD ADDRESS**CURRENT ADDRESS**

TELEPHONE NUMBER: () _____

DNA PUBLICATION NUMBER/TITLE**CHANGES/DELETIONS/ADDITIONS, etc.)**
(Attach Sheet if more Space is Required)

DNA OR OTHER GOVERNMENT CONTRACT NUMBER: _____

CERTIFICATION OF NEED-TO-KNOW BY GOVERNMENT SPONSOR (if other than DNA): _____

SPONSORING ORGANIZATION: _____

CONTRACTING OFFICER OR REPRESENTATIVE: _____

SIGNATURE: _____

CUT HERE AND RETURN



DEFENSE NUCLEAR AGENCY
ATTN: TITL
6801 TELEGRAPH ROAD
ALEXANDRIA, VA 22310-3398

DEFENSE NUCLEAR AGENCY
ATTN: TITL
6801 TELEGRAPH ROAD
ALEXANDRIA, VA 22310-3398

| REPORT DOCUMENTATION PAGE | | | Form Approved OMB No. 0704-0188 | |
|---|---|--|---|---|
| <small>Public reporting burden for this collection of information is estimated to average 1 hour per response including the time for reviewing instructions, searching existing data sources, gathering and maintaining the data needed, and completing and reviewing the collection of information. Send comments regarding this burden estimate or any other aspect of this collection of information, including suggestions for reducing this burden, to Washington Headquarters Services, Directorate for Information Operations and Reports, 1215 Jefferson Davis Highway, Suite 1204, Arlington, VA 22202-4302, and to the Office of Management and Budget, Paperwork Reduction Project (0704-0188), Washington, DC 20503</small> | | | | |
| 1. AGENCY USE ONLY (Leave blank) | | 2. REPORT DATE 940101 | | 3. REPORT TYPE AND DATES COVERED Technical 921001 - 930228 |
| 4. TITLE AND SUBTITLE Modeling the Total Dose Radiation Effects of $Hg_{1-x}Cd_xTe$ Photodiodes Using Numerical Device Simulators | | | 5. FUNDING NUMBERS C - DNA MIPR-92-501 | |
| 6. AUTHOR(S) James C. Petrosky, James W. Howard, and Robert C. Block (Nuclear Engineering and Engineering Physics), and Iswara Bhat (Electrical, Computing, and Systems Engineering) | | | | |
| 7. PERFORMING ORGANIZATION NAME(S) AND ADDRESS(ES) Rensselaer Polytechnic Institute P.O. Box 965 Troy, NY 12181 | | | 8. PERFORMING ORGANIZATION REPORT NUMBER | |
| 9. SPONSORING/MONITORING AGENCY NAME(S) AND ADDRESS(ES) Defense Nuclear Agency 6801 Telegraph Road Alexandria, VA 22310-3398 RAEE/Cohn | | | 10. SPONSORING/MONITORING AGENCY REPORT NUMBER DNA-TR-93-50 | |
| 11. SUPPLEMENTARY NOTES | | | | |
| 12a. DISTRIBUTION/AVAILABILITY STATEMENT Approved for public release; distribution is unlimited. | | | 12b. DISTRIBUTION CODE | |
| 13. ABSTRACT (Maximum 200 words) We fabricated high quality MCT diodes using in-situ grown MCT and selective annealing. We used these diodes to benchmark our initial characterization and as a basis for our irradiation modeling. We implemented the models in PISCES-IIB and compared the I-V relationship to measurements. The close match between simulations and measurements demonstrates the applicability of the models. We expanded the simulations to I-V characteristics of irradiated diodes. To do so, we developed models for the induced current mechanisms resulting from radiation interactions. The results confirm the theories concerning the radiation's effect on tunneling in MCT. The simulations also suggest that improvements require knowledge of tunneling currents associated with trap formation in MCT. | | | | |
| 14. SUBJECT TERMS Radiation Effects Infrared Detectors | | | 15. NUMBER OF PAGES 58 | |
| MCT Device Simulations | | | 16. PRICE CODE | |
| Mercury Cadmium Telluride Photodiodes | | | | |
| 17. SECURITY CLASSIFICATION OF REPORT UNCLASSIFIED | 18. SECURITY CLASSIFICATION OF THIS PAGE UNCLASSIFIED | 19. SECURITY CLASSIFICATION OF ABSTRACT UNCLASSIFIED | 20. LIMITATION OF ABSTRACT SAR | |

UNCLASSIFIED

SECURITY CLASSIFICATION OF THIS PAGE

CLASSIFIED BY:

N/A since Unclassified.

DECLASSIFY ON:

N/A since Unclassified.

SECURITY CLASSIFICATION OF THIS PAGE

UNCLASSIFIED

SUMMARY

This document summarizes our research in modeling the total dose radiation effects in $\text{Hg}_{1-x}\text{Cd}_x\text{Te}$ (MCT) Photodiodes from 1 October 1992 through January 1993. This research encompasses the initial studies in MCT growth, device fabrication, device characterization, irradiation tests, and device simulation. Our results indicate the ability to simulate MCT device performance using a numerical simulator, both before and after irradiation.

We grew MCT crystals at the Electrical, Computing, and Systems Engineering Department (ECSE) using an in-situ method known to produce nearly defect free semiconducting material. An annealing technique was used to fabricate photovoltaic diodes because it avoids producing damage in the crystal. We used these high quality diodes to benchmark our initial characterization and as the basis of our irradiation studies. This report details our growth technique, device design, and characterization.

The Nuclear Engineering and Engineering Physics Department (NEEP) used the characterization data and device physics to produce models for the electrical characteristics of the MCT diodes. We implemented these models in PISCES II-B, a two-dimensional device simulator, and compared the current-voltage (I-V) relationship of the simulations to our measurements. The close match between the simulations and measurements demonstrates the applicability of the models. We then expanded the simulations to the I-V characteristics of irradiated diodes. To do so, we developed models for the induced current mechanisms resulting from the irradiation. These too were added to the PISCES code and improved the post irradiation simulations. This report gives results of the simulations, and details the theories and models used to simulate radiation effects in MCT.

The results of this research confirm the ability to consistently grow high quality devices using an in-situ method. They also indicate the ability to model these devices both before and after they are irradiated, using models for the physical phenomena governing transport in the devices. Simulations suggest that improvements to the models will require additional data to effectively model phenomena associated with trap formation in MCT. We have already begun developing experiments to obtain the necessary data for these improvements.

TABLE OF CONTENTS

| Section | Page |
|--|------|
| SUMMARY | iii |
| FIGURES | vi |
| 1 INTRODUCTION | 1 |
| 1.1 Background | 1 |
| 1.2 Approach | 2 |
| 2 MCT DEVICE FABRICATION | 3 |
| 2.1 Epitaxial Growth | 3 |
| 2.2 Device Fabrication | 3 |
| 2.3 Device Characterization | 4 |
| 2.4 Results | 4 |
| 3 RADIATION EFFECTS IN MCT | 7 |
| 3.1 Principle Theory of Radiation Effects in MCT | 7 |
| 3.1.1 Bulk Effect | 7 |
| 3.1.2 Surface/Boundary Radiation Effects | 11 |
| 3.2 Radiation Effects Experiments | 14 |
| 4 SIMULATIONS | 17 |
| 4.1 PISCES-IIB | 17 |
| 4.2 Modeling MCT Device Characteristics - The First Step | 19 |
| 4.3 Modeling the Tunneling Phenomenon | 22 |
| 5 CONCLUSIONS | 29 |
| 6 REFERENCES | 30 |

TABLE OF CONTENTS (Continued)

Appendix

| | | |
|---|---------------------------|-----|
| A | SUBMITTED PAPERS | A-1 |
| B | RADIATION TEST PLAN | B-1 |

DTIC QUALITY INSPECTED 2

| | |
|--------------------|-------------------------------------|
| Accession For | |
| NTIS GRA&I | <input checked="" type="checkbox"/> |
| DTIC TAB | <input type="checkbox"/> |
| Unannounced | <input type="checkbox"/> |
| Justification | |
| By | |
| Distribution/ | |
| Availability Codes | |
| Dist | Avail and/or Special |
| A-1 | |

FIGURES

| Figure | | Page |
|--------|---|------|
| 2.1 | Measured photoresponse curves | 5 |
| 2.2 | R_0A measured for several devices | 6 |
| 3.1 | CdTe mean displacement energy compared to other semiconductors..... | 9 |
| 3.2 | The nearly equal shift in the flatband voltage away from the zero point indicates both electron and hole trapping at the boundary..... | 12 |
| 3.3 | Relationship between current and dose for irradiated diodes at different reverse biases | 14 |
| 4.1 | Original forward bias I-V PISCES simulations compared to measured data | 20 |
| 4.2 | Original reverse bias I-V PISCES simulations compared to measured data | 20 |
| 4.3 | Calculated vs. measured n_i | 22 |
| 4.4 | Forward bias simulations after modifications | 23 |
| 4.5 | Reverse bias simulations after modifications..... | 23 |
| 4.6 | Reverse bias energy band diagram showing the potential barrier..... | 24 |
| 4.7 | A Boltzman function fit to data..... | 26 |
| 4.8 | Reverse bias simulation of a P-N junction with and without the tunneling models..... | 27 |
| 4.9 | Results of simulated radiation effects compared to measured data from irradiated diodes | 28 |

SECTION 1

INTRODUCTION

Recent shifts in strategic defense require space borne monitoring, tracking, and targeting of long range missiles using their IR signatures. This application implies MCT use in an aggressive space and weapons generated radiation environment. Detailed knowledge of the effects of ionizing radiation is essential for predicting future response changes and to develop devices that are radiation hardened.

The vulnerabilities of MCT photodiodes in space applications and changes in response of detectors after radiation exposures have generated concern over the mechanisms of radiation damage in MCT devices. There is a need to predict their behavior in this harsh environment. Some knowledge of the bulk and surface radiation effects exists, but current theories cannot accurately predict the response of MCT devices to radiation. Additionally, a better understanding of the mechanisms of radiation effects may help to improve the quality and hardness of future MCT devices.

Currently the effects of radiation cannot be predicted on general device structures a priori. Instead researchers and manufacturers use trial and error studies to find the extent of damage. This method often proves to be misleading because parametric dependencies are vastly different based on scaling and manufacturing techniques. A device simulator would prove useful in the study of radiation effects in MCT devices, provided the models were predicated on material parameters that can be measured and have consistent dependencies.

The major difficulty with developing such a device simulator is that until recently, MCT diodes could not be produced pure enough to separate the junction and tunneling currents. Because of this, simple device characterization becomes very complicated. This leads to inaccuracies in the proper device characteristics, prior to adding the complications induced by the radiation damage.

1.1 BACKGROUND.

MCT is a direct band gap semiconducting material belonging to the II-IV chemical groups. It has a tunable band gap that varies almost linearly with the change in the composition variable, x . HgTe is a semimetal with a band gap of around - 0.3 eV whereas CdTe is a semiconductor with a bandgap of 1.605 eV.

Since its discovery in the late 1950s as an infrared (IR) detector material, the scientific and military communities have given much attention to MCT. In the early 1960s with the arrival of satellite technology, it became necessary for IR detectors in space to respond in the 3-5 and 8-14 μm spectral windows and operate at liquid nitrogen temperatures. MCT is one of few semiconductors that operate in this range. Its tunable band gap and high quantum efficiency made it the premier material for this application. Since then, much of the effort in MCT research was directed at growth and characterization of MCT devices with $0.2 < x < 0.4$. This corresponds to IR response in the CO_2 and H_2O non-absorption edges, which are most important for military satellite sensor systems. Not until the last decade has the technology been available to produce high quality MCT, making them a commercially available IR detector.

1.2 APPROACH.

Our modeling approach is unique since its foundation is growth and modeling of relatively pure devices. These steps are absolutely necessary to ensure that device simulation accurately portrays the intrinsic electrical characteristics of the device. Once this is accomplished, we add models for radiation induced tunneling with reasonable assurance that the electrical characterization is accurately modeled. Until recently, devices of sufficient purity were not able to be grown. However, advancements in organometallic vapor phase epitaxy (OMVPE) technology and selective annealing have resulted in MCT devices with I-V relationships which approach ideal limits. Since this device manufacturing method is being explored at Rensselaer Polytechnic Institute (RPI), device characterization and design parameters are well known for irradiation and modeling purposes.

SECTION 2

MCT DEVICE FABRICATION

2.1 EPITAXIAL GROWTH.

We grew all MCT layers by organometallic vapor phase epitaxy (OMVPE) using the direct alloy growth (DAG) technique. This method provides precise control over the elemental mercury content of the material during growth, without requiring high temperatures. By growing the MCT layer epitaxially on CdTe, we do not reduce the response of the MCT active layer since CdTe has a larger band gap than MCT. The close lattice match and stoichiometric similarities produce a nearly defect free interface.

The OMVPE growth also lends itself to the in-situ placement of the CdTe passivation. Since the constituents of the MCT growth can be varied in the reactor, the elimination of elemental mercury results in growth of CdTe. Therefore the mercury is simply evacuated from the reactor after the appropriate growth period and then CdTe growth begins on top of the MCT layer. The CdTe again forms a nearly defect free interface, and also serves a mask during device fabrication.

2.2 DEVICE FABRICATION.

We fabricated a number of photodiodes during the course of this work. The as-grown layers were p-type with carrier concentrations around $4 \times 10^{16} \text{ cm}^{-3}$ due to Group II vacancies. A P-N junction was formed by opening an array of windows in the CdTe cap and then annealing the layers under saturated Hg overpressure. This process, called selective annealing, converts the entire MCT layer under the windows to n-type. The n-type region formed 600 μm diameter cylindrical junctions in the p-type material. Indium dots were used to make n-type contacts, while gold was used to contact the p-type MCT.

We packaged the samples in a 22 pin flat-pack, and cut a rectangular window slightly smaller than the sample size to facilitate backside illumination of the photodiodes. The sample was fastened to the flat-pack using epoxy. The other ends of the gold wires were also attached to flat-pack pins using epoxy, completing the fabrication and packaging of the devices.

2.3 DEVICE CHARACTERIZATION.

We characterized the photodiodes by their current-voltage (I-V) characteristic, R_0A , and spectral response. I-V was measured at 77°K using a transistor curve tracer. This was done by using a pair of microprobes while the device was immersed in liquid nitrogen. I-V characteristics under the 295°K (room temperature) background as well as the 77°K (thermal equilibrium) background were measured in this manner. The latter was done by covering the flat-pack using a thin indium foil which was also immersed in liquid nitrogen.

The sample was then mounted on the cold finger of a cryostat. The flat-pack was kept pressed against the cold-finger using a copper plate, which also provided a thermal equilibrium background for the devices. A thin indium foil was used between the flat-pack and the cold finger to assure a good thermal contact. Coaxial cables were used for connecting the flat-pack pins to the electrical connections on the Dewar. The samples were cooled down to 77°K, and the dynamic resistance and I-V of the device measured. A signal generator was used to provide the voltage sweep necessary for this measurement. The voltage sweep rate was typically about 1 mV/second. The dynamic resistance was measured using a log picoammeter. The I-V of the device around zero bias was measured using an electrometer and the data recorded on an x-y plotter. Following these measurements at 77°K, we gradually warmed the devices to room temperature. During this warm up period, we measured I-V as a function of temperature.

We measured the spectral response of the device in the 2.5 to 14 μm range using an IR source equipped with a 50 Hz chopper and a monochromator. For this purpose, the device was mounted in a liquid nitrogen cooled Dewar equipped with an IR transparent ZnSe window. The flat-pack was kept pressed against the cold finger using a copper plate, which had a rectangular opening in the middle to allow IR transmission. The spectral response was measured under a short-circuit condition, using a current pre-amplifier, the output of which was coupled to a lock-in amplifier. The lock-in frequency was the frequency of the chopper on the IR source. The incident photo flux on the device was measured by replacing the device by a standard detector and measuring its response.

2.4 RESULTS.

The most significant result of our growth studies is that we have our MCT OMVPE reactor back on line, have begun growing MCT, and are making devices. There is one student dedicated to research on intrinsic growth methods and device fabrication in MCT,

and another student is exploring advanced methods in MCT device designs using extrinsic dopants.

The skills required for our OMVPE growth research have developed rather quickly. Within three months our devices are nearing the quality of those done in previous research: skill which previously took years to develop. Additionally, we are focusing our work on the more difficult problem of growing MCT with a lower x than our previous research, with a goal of manufacturing high quality diodes which respond in the 10-15 μm range ($0.18 < x < 0.24$). With the initial learning curve behind us, we expect even higher quality devices in the near future.

Figure 2.1 shows the spectral response curves for two diodes at 77K under constant photon flux, for the case of front side illumination. The cutoff wavelength is the wavelength where the photoresponse reaches $\frac{1}{2}$ the peak value. Carriers are collected across the vertical junction within a diffusion length. Since the electron diffusion length is much larger than for holes, it is the dominant carrier. A flat curve implies low recombination velocities and long diffusion lengths.

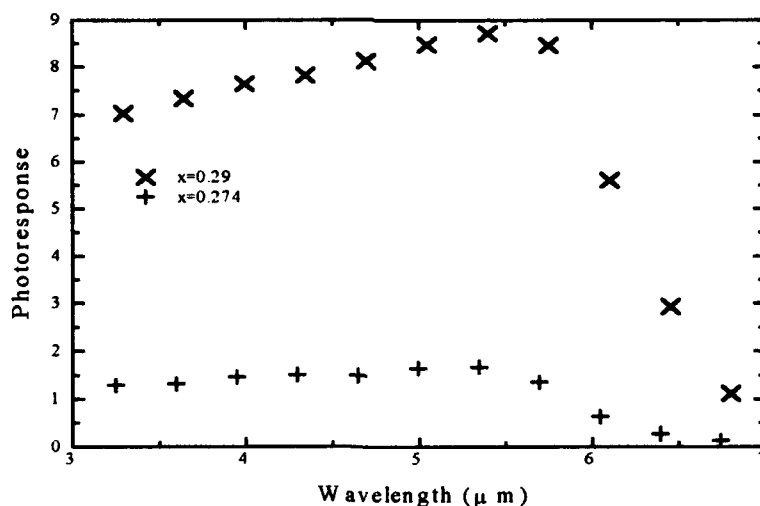


Figure 2.1. Measured photoresponse curves. The photoresponse is measured in units of $\mu\text{A}/\text{cm}^2/\text{s}/\text{photon}$.

Figure 2.2 shows the R_0A product for our recent MCT devices, compared to our earlier work¹ and Sarusi. The difference in R_0A is as expected since it is less for a smaller x value. However the shape suggests a leakage across the surface of the device. This may be due to mechanical defects at the MCT/CdTe which form during growth, or due to leakage caused by the formation of the n side contact. The R_0A is still larger than those for LPE, demonstrating that the device is still of "good" quality.

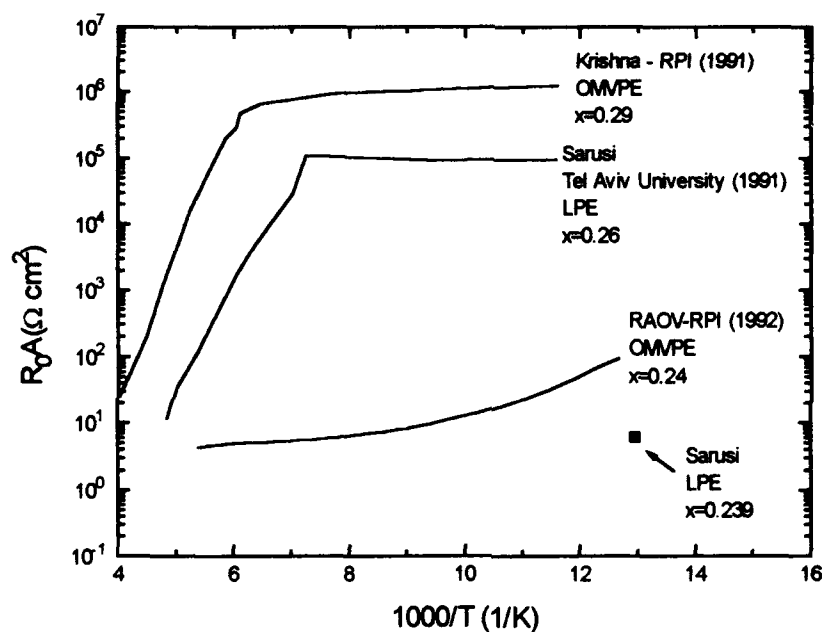


Figure 2.2. R_0A measured for several devices.

¹Krishina was previously at RPI studying MCT growth by OMVPE. Raov is currently researching OMVPE growth at RPI.

SECTION 3

RADIATION EFFECTS IN MCT

Our radiation effects research began with a thorough investigation into the available literature. We analyzed the results and conclusions found in this literature with respect to our knowledge of radiation damage mechanisms. We then tested the models and theories using simulations and derived our own conclusions and models. One conclusion is that additional experiments are needed to improve upon the models we developed. The radiation effects modeling is therefore categorized into three areas: (1) understanding the physical theories governing the effects, (2) constructing models for the irradiation effects and simulating, and (3) conducting radiation experiments to confirm simulation results or gain additional data. This section will cover items one and three. We will cover item two in section, where we present results of our simulations.

3.1 PRINCIPLE THEORY OF RADIATION EFFECTS IN MCT.

The effects of ionizing radiation on MCT devices are complicated. Passage of radiation changes the electrical transport properties in the insulator/passivant layer, and can also free atoms that quickly diffuse through the bulk. Finding the scope and effect of these changes is even more difficult because abnormalities in the device and intrinsic damage can mask any notable experimental changes. For that reason, an understanding of the effects of radiation in MCT is still in its infancy. Since device physics is still the same as in other semiconductors, we can infer much of the theory from knowledge of devices made from other materials.

3.1.1 Bulk Effect.

Bulk effects in MCT occur as the radiation imparts its energy to the Hg, Cd and Te bonds in the device. The effect of breaking the bonds allows for the thermal diffusion of any of the elements from its location to another energetically favorable site. Given the low bond strength of Hg and its high diffusion constant, it is the main contributor to bulk radiation effects. The diffusion becomes most important at P-N junctions and interfaces because built in electric fields remove the randomness of the Hg atom motion and make them less likely to move back to their initial position. Table 3-1 shows the energy levels and diffusion constants for Hg and Cd in MCT.

Table 3-1. Bulk radiation effect parameters.

| | Diffusion Constant ² (cm ² /sec) | Vacancy Energy (eV) |
|---------|---|---------------------|
| Mercury | 4.5x10 ⁻¹¹ | 2.2 |
| Cadmium | 5.6x10 ⁻¹⁷ | 4.7 |

Hg diffusion has two effects on the electrical characteristics of the device. First, the removal of the Hg causes the material to have fewer donors and thus causes a material type change, as discussed in section 2. This changes the way in which the junction functions when forward or reverse biased. Comparing the energy for creation of a Hg vacancy with the absorbed dose gives an upper limit to the number of vacancies created by the incident radiation. Here, the sample is 0.5 cm² and 10 μm thick. With 200 krad absorbed dose, all energy going into Hg bond breaking, and Hg not returning to sites previously occupied by Hg atoms (upper limit case), the total change in donor population will be:

$$2 \times 10^5 \text{ rad} \times \frac{6.24 \times 10^{13} \text{ eV/g}}{\text{rad}} \times \frac{8.5 \text{ g}}{\text{cm}^3} \times \frac{\text{vacancies}}{2.2 \text{ eV}} = 4.8 \times 10^{19} \text{ cm}^{-3} \quad (3.1)$$

It is highly unlikely that the upper limit assumption would be valid. However with doping limits nearly two orders of magnitude below ($\sim 10^{17} \text{ cm}^{-3}$) the Hg diffusion may still dominate the junction. We found no data in our literature search that presents carrier concentration change due to low total doses of irradiation. Research in this area is a part of our experimental analysis.

Second, the Hg (and in a small way Cd) can create carrier traps as they find energetically favorable positions not previously occupied by the same atom. The carrier traps add significant leakage currents across the junction through the trap assisted tunneling (TAT) mechanism. The amount of the TAT depends on the concentration and energy level of the carrier traps.

If the incoming radiation particle has non zero mass, displacement damage can also occur due to elastic collisions. The energy required to displace the atom from its site is

²These values are for 450 °K and Hg pressure of $\sim 10^5$ Pa [2].

called the displacement damage threshold energy (T_d). Theoretical calculations of T_d show it is dependent upon the reciprocal of the crystal lattice constant as shown in figure 3.1. Since the lattice constant varies less than 3% from CdTe to HgTe, T_d for MCT is around 6.6 eV.

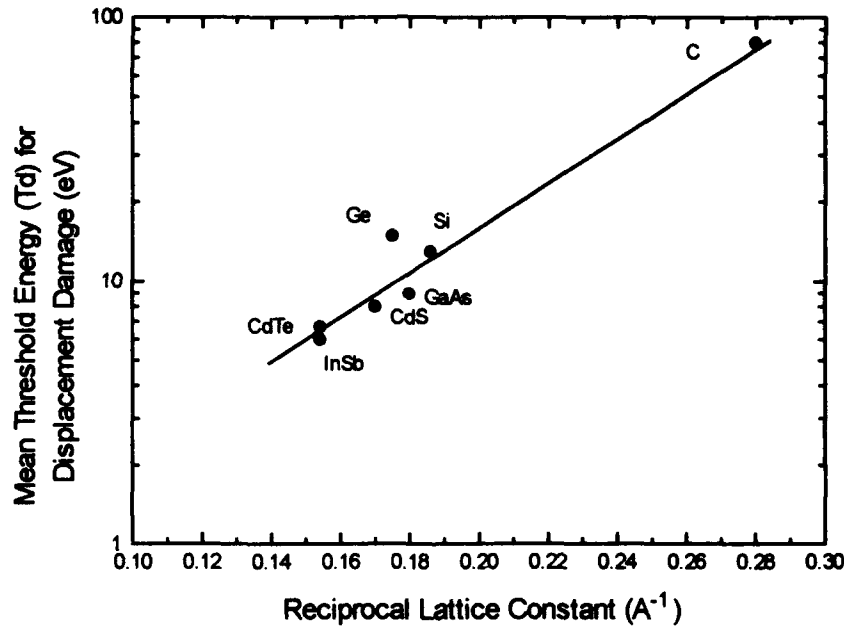


Figure 3.1. CdTe mean displacement energy compared to other semiconductors.

The maximum number of defects produced can then be calculated using

$$N_d = \left(\frac{6 \ln 2}{\pi^2} \right) \left(\frac{T_{rd}}{T_d} \right) \quad (3.2)$$

where T_{rd} is the recoil energy expended in the displacement process. As a rough estimate, if 200 krad of 1MeV electrons pass through 10 μm of MCT, approximately 10^{10} displacements can be formed.

The vacancy can influence the displaced particle and cause it to return to its original site unless the particle has sufficient energy to move away from its influence. In this way the damage is self corrected, or annealed. If the displaced particle has a great amount of additional kinetic energy, or is influenced by a potential difference, it may move away from the vacancy site. The most probable outcome is for it to produce a *Frenkel defect*, where

the atom leaves the vacancy behind and moves into a lattice interstitial site. Both the vacancy and interstitial create a trapping site for charge carriers, reducing the carrier lifetime.

The displaced atoms also change the periodicity of the lattice potential, forming energy states that can be electrically active. Their presence can change the general performance of the material. If there are more electrically active donor sites, the material becomes more n-type.

Ion implantation studies reveal that damage induced by ion implantation increases the donor population despite the implanted species (donor, acceptor, neutral), causing a p to n type conversion. This means that the donor population increases more rapidly than the acceptor population. The actual nature of the donor site is unknown at this time but is believed to be a Te vacancy or a Hg antisite on a Te vacancy. Additionally, ionized species of Te and Hg exist due to radiation induced ionization. These may produce complexes by occupying the Hg or Te vacancy sites.

Electron irradiation studies of bulk MCT confirms the creation of donor levels and suggests their energy levels. D. G Morral used Hall measurements to characterize changes due to 30 MeV electron irradiation of bulk p-type MCT wafers. He found that at $\sim 295^\circ\text{K}$ p to n type conversion occurred after a dose of $6 \times 10^{15} \text{ e}^-/\text{cm}^2$. Lowering the temperature reversed the effect. The conversion did not occur at low temperatures ($< \sim 240^\circ\text{K}$). This observation is consistent with Malon et al. who also observed p to n type conversion for various other stoichiometries.

Donor freeze-in implies a deeper level for the donor defects than the shallow Hg acceptor levels. Using Morral's conductivity diagrams and assuming the reduced conductivity is a result of the n to p type conversion at 238°K , the donor level should be around 20 meV below the conduction band. Since a one-to-one ratio of Hg vacancies to interstitials is at best possible with no Hg loss, the donor level may involve the neutralization of Hg vacancy defects as complexes.

Radiation affects the bulk through formation of Hg and Te interstitial and vacancy sites. Both radiation induced bond breaking with thermal/electric field enhanced motion and collisions with incoming particles form these sites. The Hg vacancies are acceptor sites, while the Hg interstitials are donors. Reversible n to p type conversion at high temperatures suggests that a donor level be created which dominates at high temperatures,

but is frozen in at lower temperatures. The actual constituents of the donor defects have not yet been identified.

3.1.2 Surface/Boundary Radiation Effects.

The most prominent effects of ionizing radiation in MCT occur at the surface and boundary layers. Ionizing radiation can degrade device performance by increasing trapped charge in the passivation layers surrounding the P-N junction. This ultimately results in increased tunneling currents across the junction.

Surface radiation effects can occur from lasers, γ rays, or from incident charged particles. Each has the same result. Passage of radiation ionizes the atoms in the insulator. Then free electrons and holes move by diffusion or a potential difference to the surface boundaries where they can be trapped at energetically favorable sites. These sites occur because of the lattice mismatch at the boundary, stoichiometric differences in the material, or impurities. Additionally, free charges on the MCT side of the boundary may tunnel through the boundary and become trapped as well. The result is a buildup of charge in the insulator/passivant and/or a loss of charge at the surface of the semiconductor that may cause the bands to bend. If sufficient band bending occurs at the surface, tunneling currents can become the dominant factor in the junction currents.

Surface effects are tested using two methods, metal-insulator-semiconductor (MIS) flatband voltage, and current voltage (C-V) and diode I-V measurements. There is general agreement in the literature regarding radiation effects at the surface using either of these methods.

MIS flatband experiments help identify the type of charge carrier that becomes trapped along the boundary. Device C-V measurements show the preexisting boundary charge density. The device is then irradiated with a gate bias. C-V measurements are then used to find the required voltage to reestablish flatband conditions. The charge density at the surface is then found. A positive bias on the gate during irradiation places positive charge carriers or holes at the boundary. If a flat band voltage shift occurs then the result is due to electrons crossing the boundary. If the same experiment is done using a negative bias, the opposite is true. MCT flatband experiments reveal a nearly equal flatband voltage shift for positive and negative gate biases during irradiation (figure 3.2), meaning both holes and electrons get trapped and the trapping process may involve several yet unknown species.

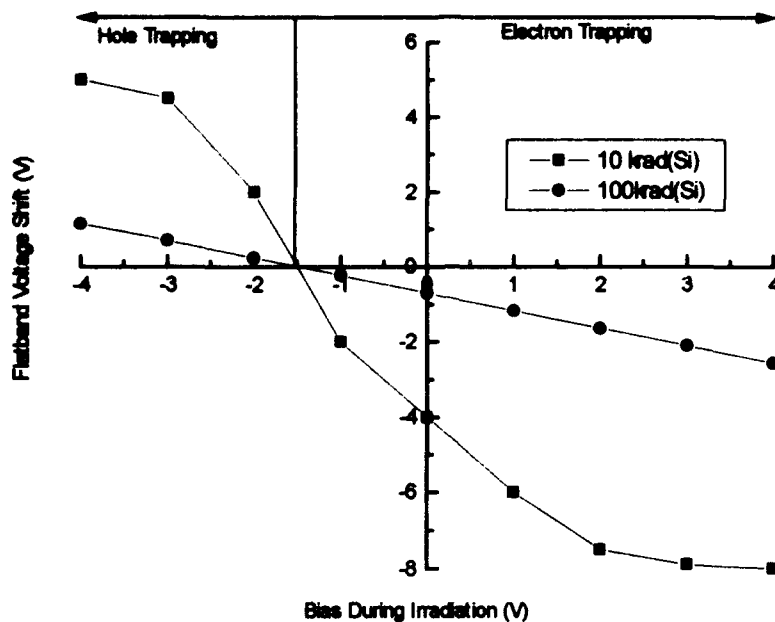


Figure 3.2. The nearly equal shift in the flatband voltage away from the zero point (-1.4V) indicates both electron and hole trapping at the boundary.

The flatband voltage measurement also reveals the effectiveness of the charge traps at the surface. In MCT/ZnS boundaries, there is considerable charge loss in the insulator due to recombination of the electrons and holes. The e-h pairs required to produce the observed flatband voltage shift shows that there can be up to a 97% charge loss due to e-h recombination at high electric fields ($\sim 3 \times 10^5$ V/cm) which is very device dependent. This makes it extremely difficult to know *a priori* how much charge becomes trapped.

Bias switching and annealing studies also reveal that biasing or thermal annealing reverses the surface trapping phenomenon. During bias switching studies, the switching makes charge available which recombine with the traps. This removes nearly all of the trapped charge carriers.

The increased charge at the surface produces conduction channels at the surface. However, the number of carriers may not just be a result of the intrinsic excess charge. Irradiated diodes have currents that exhibit a weak dependence on temperature. This suggests that the channel conduction mechanism may be tunneling. If so, the tunneling

current would show a dependence on the electric field caused by both the applied voltage and the surface states by the equation:

$$\log(I) = C - \frac{A}{E_j} \quad (3.3)$$

$$E_j = \frac{(Q_a + Q_i)}{\epsilon \epsilon_0}$$

where:

C and A are constants

E_j is the junction electric field

Q_a is the charge resulting from the applied voltage

Q_i is the charge contributed by the surface states produced by radiation.

ϵ is the relative permittivity of the semiconductor

ϵ_0 is the permittivity of free space.

If the surface states produced by radiation are proportional to dose, then the reverse current should exhibit a linear dependence on the dose. Figure 3.3 shows a typical case where this dependence is generally followed. Deviation from linearity may be the result of increases in surface recombination velocities as reported by Bajaj et al.. These results show that a simple current relationship may not be appropriate for surface currents in irradiated MCT devices.

Annealing studies done with and without a bias reveal that the bias induced electron injection across the boundary does not contribute to the reduction of charge at the surface. Instead there is a dependence on the annealing temperature only, which suggests the presence of a thermally dependent detrapping mechanism. Studies of both MIS and diodes reveal that the surface density of trapped charge returns to its initial value after annealing at room temperature, though the deep level complex traps remain.

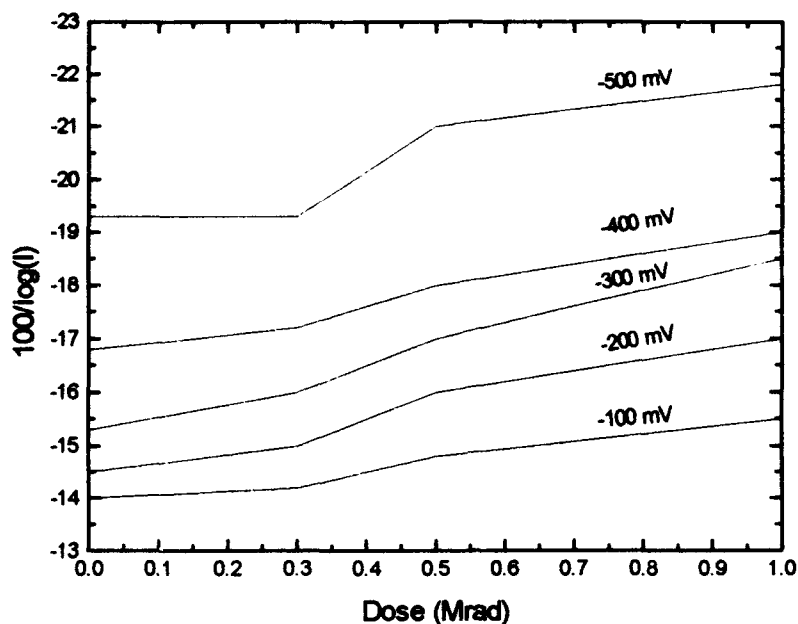


Figure 3.3. Relationship between current and dose for irradiated diodes at different reverse biases.

3.2 RADIATION EFFECTS EXPERIMENTS.

Although literature data helps provide insights to form a basis for our modeling efforts, we need experiments specific to our work to provide the necessary information for our modeling. In particular, we need information regarding the doping levels, mobility, and trap energy level and concentrations as a function of dose for our diodes. Our experiments must be done under controlled temperature conditions to avoid changing the results of irradiation by annealing. Additionally, the diodes we use as a basis have very low reverse bias leakage with saturation currents in the 10 femptoamp to picoamp region. This means that our I-V data collection equipment must be sensitive in the near theoretical limits of measurement. A copy of our radiation test plan is in appendix B.

All radiation effects experiments and measurements will be done by incrementally irradiating MCT devices or samples cooled by liquid nitrogen in a dewar. Once cooled, the devices must remain at this temperature (77°K) until the radiation measurements are complete. This is done to reduce the effect of thermal annealing on the parameters of interest. Traps associated with interstitials anneal at temperatures above 150°K.

As the temperature decreases, the time for carrier movement and trap formation increases. We expect this to be on the order of seconds to minutes. Therefore time for carrier movement and trap formation must be given after each irradiation. We will find the formation time by irradiating a device in the dewar system and measuring I-V at various post irradiation times and for the extreme bias conditions of interest to us (-2 to 2 V). This will be done at several irradiation levels. We expect that there will be an initial incremental change in the current vs. time plot, which shows stability after a time, T_s . All subsequent measurements must be taken after T_s to provide consistency in the experiments.

Hall effect measurements provide a measure of sample carrier concentration and mobility by measuring the sample sheet resistance in a magnetic field. Since the concentration and mobility directly affect the I-V characteristics of the device, Hall effect measurements can be used. We will investigate the carrier concentration dependence by irradiating n and p type samples and then conducting Hall measurements on them to find carrier concentration changes. The temperature will be maintained at 77°K by irradiating and measuring in a dewar. The n and p samples must have initial carrier concentrations equal to the diodes that we are simulating. In this way we can separate carrier changes as a function of dose for both the n and p side. We can also find the majority carrier mobility dependence as a function of dose. Our Hall effect measurements are made using a portable measurement system with a 3440 gauss cesium magnet. The measurement is computer controlled, and calculates the concentration and mobility directly.

Deep level transient spectroscopy (DLTS) can provide information about deep level trap energy levels and concentration by using current pulse measurements and current switching at various temperatures. In the same way as with Hall effect measurements, we can measure n and p type samples using DLTS to learn the trap levels and trap energy levels as a function of dose. However, since the measurement requires variation in temperatures a dewar system is inadequate. Instead, we must use a cryogenic system that can be in the radiation environment and have temperatures varied below 150°K.

Finally, the I-V characteristics of diodes directly link the measurements to our simulation results. Our experiments will include irradiating diodes in a dewar system and measuring the I-V characteristic. Measurements will be done using a Keithley source measurement controlled by a computer, which will log I-V relationship and time of the measurement. A triax cable linked to a shielded dewar system reduces the noise in the measurement system. The source voltage will be varied from -2 to 2 volts in 20 mV increments, and two measurements done for each radiation increment to investigate any

possible detrapping that may occur because of the measurements. We expect currents between 0.1 picoamps and milliamps, which is within the capabilities of the measurement system.

SECTION 4

SIMULATIONS

Incorporating MCT devices into a simulator should be a straight forward process. However, until recently the only MCT devices by which we could gauge proper model performance displayed phenomena which were difficult to model. Hence, the fundamental device characteristics remained masked, while modeling focussed on other phenomena. If we remove the effects of these phenomena through technological growth and design advancements (as discussed in section 2), then modeling the characteristics once again becomes straight forward. After this point, we can include the additional phenomena since the radiation tends to enhance them.

Device simulators are quite useful for studying semiconductor devices and circuits. They provide valuable information for device designers, material researchers, and those investigating the effects of various environments on devices. Researchers prefer using simulators because of their low cost (in comparison to manufacturing and experimental analysis), ease of control, or when it is impractical to retrieve a device already in operation (such as a sensor array on a satellite). PISCES is one of several device simulators used by researchers, and is considered the "industry standard" in most forums. The following sections cover PISCES-IIB, the initial MCT diode characteristic modeling, and radiation effects modeling using a tunneling model.

4.1 PISCES-IIB.

PISCES-IIB (PISCES)³ is a two dimensional semiconductor device analysis tool based on the self consistent solution of the Poisson and carrier continuity equations. The code offers a variety of analysis tools for evaluating device characteristics, and most can be changed without modifying the code. One can select the device geometry, semiconductor composition, insulators and up to ten electrodes. Specific material parameters can be input, or default values used.

The governing equations solved by PISCES are given by:

$$\begin{aligned}\epsilon \nabla^2 \psi &= q[(n - p) + (N_a - N_d)] - \rho_F \\ \frac{\partial p}{\partial t} &= \frac{1}{q} \nabla J_p - U_p \\ \frac{\partial n}{\partial t} &= \frac{1}{q} \nabla J_n - U_n\end{aligned}\tag{4.1}$$

³The version used in this study was mod IIB, hereafter referred to as PISCES.

where:

Ψ is the electrostatic potential established by the charges in the device,

q is the electric charge,

ϵ is the material permittivity,

p and n are the electron and hole concentrations,

N_d and N_a are the space charge concentrations,

ρ_f is the fixed charge density found in insulating materials,

U_n and U_p are the transition or recombination terms for electrons and holes.

J_n and J_p are the electron and hole current per unit area, given by addition of their drift and diffusion components in the equation:

$$\begin{aligned} J_n &= q(\mu_n E_n n + D_n \nabla n) \\ J_p &= q(\mu_p E_p p + D_p \nabla p) \end{aligned} \quad (4.2)$$

The above equations are applied to the device by using a discretization routine which fits a grid of triangles or rectangles to the problem. Each point on the grid becomes a solution point for the above coupled equations, and each must satisfy all of the requirements for the equations and any conditions specified by each of its neighboring points.

The solution is found by placing the 3x3 matrix equations into a much larger matrix representing the entire device being simulated. Derivatives are found using a finite difference scheme, and an iterative method (Newton or Gummels) used to find singular solutions to r , p and ψ .

The programs accounts for other processes which affect n, p and ψ aside from the obvious material parameters. Most notably are recombination mechanisms. PISCES includes both Schokley Read Hall (SRH), and Auger recombination.

The SRH expression used in PISCES is:

$$U_{SRH} = \frac{pn - n_{ie}^2}{\tau_p \left[n + n_{ie} \exp\left(\frac{E_t - E_i}{kT}\right) \right] + \tau_n \left[p + n_{ie} \exp\left(\frac{E_i - E_t}{kT}\right) \right]} \quad (4.3)$$

where:

k is Boltzmann's constant,

T is temperature in $^{\circ}\text{K}$,

n_{ie} is the effective intrinsic concentration,

E_i is the intrinsic Fermi energy,

E_t is the trap energy level,

and τ_n and τ_p are the electron and hole lifetimes.

E_t equal to zero corresponds to a deep level trap at midgap, or the smallest value of the exponential term in the denominator of equation 4.3. This maximizes the SRH recombination and is sufficient to account for most SRH recombination processes, such as trap assisted and trap to trap recombination.

The PISCES Auger recombination model combines all of the possible Auger recombination mechanisms into one equation:

$$U_{\text{Auger}} = c_n (pn^2 - nn_{ie}^2) + c_p (np^2 - pn_{ie}^2). \quad (4.4)$$

The constants c_p and c_n account for the change in lifetime due to the various Auger mechanisms, while the coefficients pertain to the carrier concentration effecting Auger recombination.

4.2 MODELING MCT DEVICE CHARACTERISTICS - THE FIRST STEP.

Initial I-V simulations of MCT diodes using PISCES produced a three order of magnitude difference between the measurements and simulations. Forward bias results are shown in figure 4.1 and the reverse bias in figure 4.2.

An initial investigation revealed that several PISCES models needed modification to produce parameters necessary for MCT simulation. We modified PISCES by adding models for MCT energy gap, intrinsic concentration, and band density of states. These are needed since they deviate greatly from the PISCES parameter calculations and demonstrate a strong dependence on the composition (x) and temperature (T). They are applicable to $0.2 < x < 0.4$ and $70 < T < 150^{\circ}\text{K}$ and for bias at $-60 < V < 120$ mV. In this region tunneling currents across the pn junction are negligible. We also included 17 material parameters which are constant over the required range. Below, we highlight the most important changes.

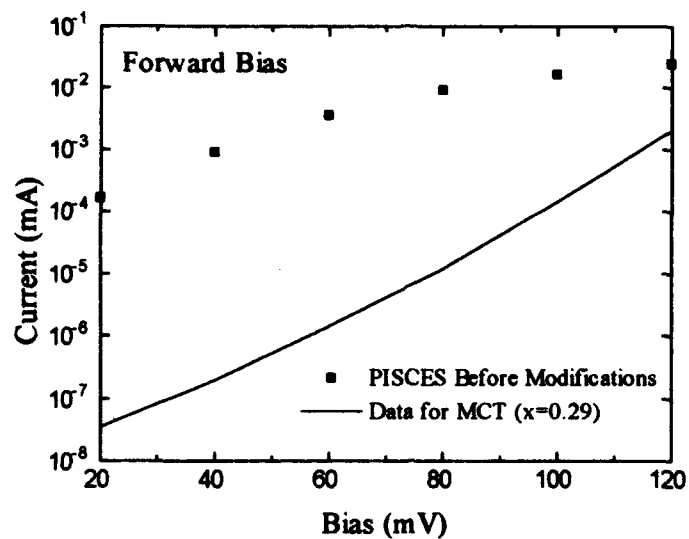


Figure 4.1. Original forward bias I-V PISCES simulations compared to measured data.

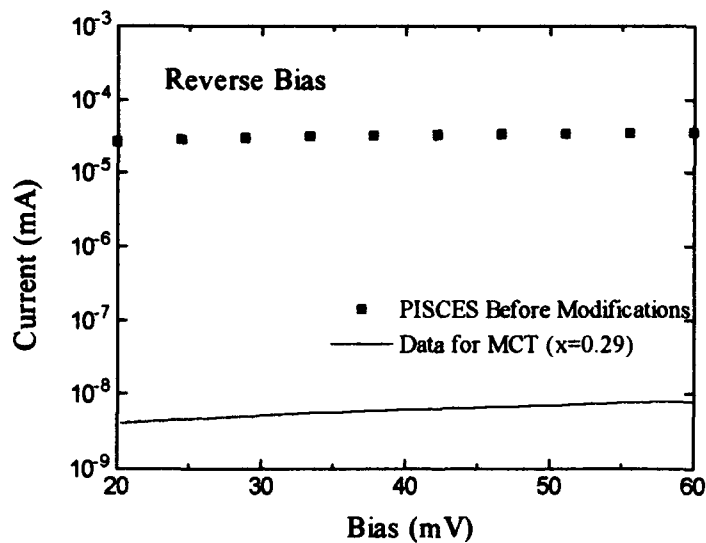


Figure 4.2. Original reverse bias I-V PISCES simulations compared to measured data.

PISCES uses a standard relationship for the intrinsic concentration derived from the mass action law and the electron and hole densities, given by:

$$n_i(T) = \sqrt{N_c N_v} e^{-\frac{E_g}{kT}} \quad (4.5)$$

In MCT, n_i has a strong dependence on x through its relationship with the energy gap and effective electron mass. These both depend on x and T . The relationship is:

$$n_i(x, T) = F \frac{(\pi\beta)^{-1/4}}{4} \left(\frac{m_n^*(x, T) m_{HH}}{m_0^2} \right)^{1/4} e^{-\beta E_g(x, T)/2} \quad (4.6)$$

$$\beta = \frac{1}{kT}$$

where:

F is a fitting parameter in atomic units,

m_0 is the electron rest mass,

$E_g(x, T)$ is the band gap energy,

m_{HH} is the heavy hole effective mass,

and $m_n^*(x, T)$ is the effective density of states.

Madarasz found good agreement between this model and experiment using $m_{HH} = 0.55 m_0$. $m_n^*(x, T)$ is given by:

$$m_n^* = \frac{m_0}{\text{den}} \quad (4.7)$$

$$\text{den} = -0.6 + 6.33 \left(\frac{2}{E_g(x, T)} + \frac{1}{E_g(x, T) + 1} \right)$$

We determined F by comparing measured values of n_i for $x = 0.2, 0.3$, and 0.4 , and $77 < T < 350^\circ\text{K}$. The error was analyzed using the chi-squared method over these ranges, and $F = 1.9 \times 10^{23}$ produced the smallest error. Figure 4.3 demonstrates how the model compares with experimental data.

The unmodified PISCES also incorrectly calculates the conduction and valence band density of states (N_c and N_v) for MCT. MCT density of states have x and T dependencies through the effective electron and holes masses as shown in equation 4.7, and the relationship:

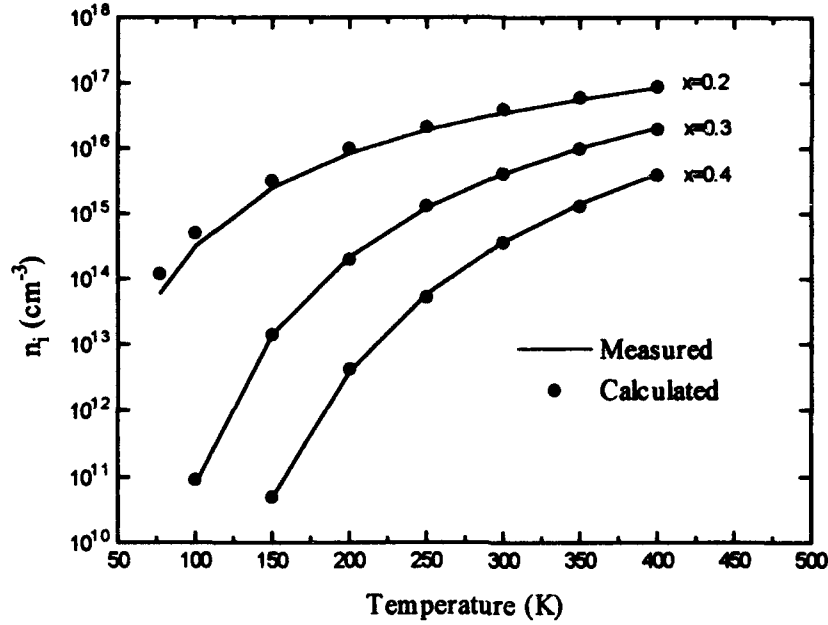


Figure 4.3. Calculated vs. measured n_i .

$$N_c(x, T) = 2 \left(\frac{2\pi m_n^*(x, T) kT}{h^2} \right)^{3/2} \quad (4.8)$$

where h is Plank's constant. For narrow band gap semiconductors [2,12], N_v equals N_c .

Figures 4.4 and 4.5 show results of simulations following the modifications. These show excellent agreement between simulation and measurements.

4.3 MODELING THE TUNNELING PHENOMENON.

PISCES lends itself easily to modeling radiation effects in MCT. This is because the dominating effects are related to carrier transport after the radiation causes charge trapping or forms charge traps. As discussed in section the trapped charges induce band bending which eventually inverts the surface. The simple band bending then leads to quantum mechanical tunneling.

PISCES allows for fixed surface charge at interfaces and junctions, which then changes the boundary conditions in the matrix equations at the boundary nodes. The fixed charge will then bend the bands to meet the tunneling requirements.

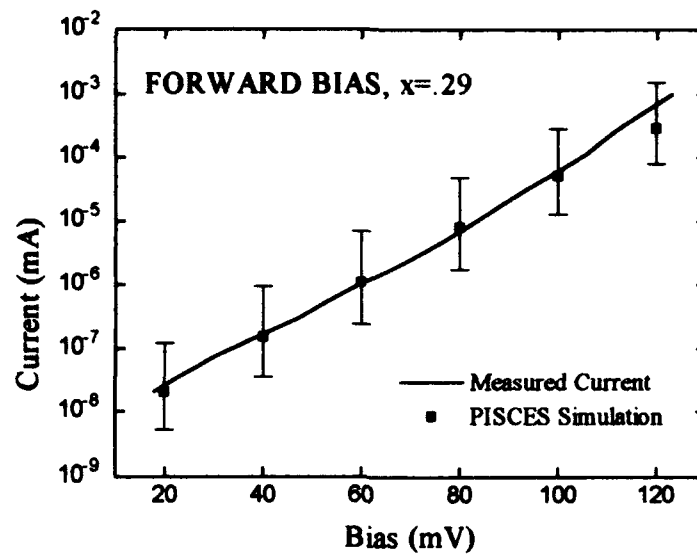


Figure 4.4. Forward bias simulations after modifications.

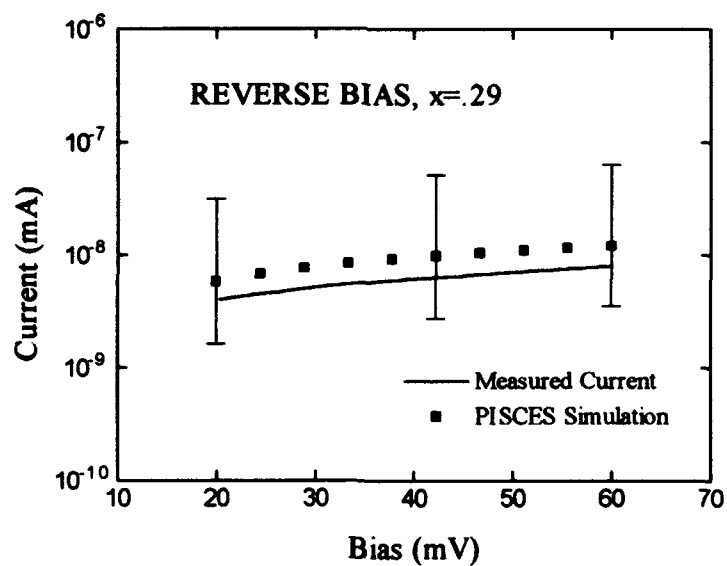


Figure 4.5. Reverse bias simulations after modifications.

The surface state density required to reach weak and strong inversion is given by:

$$Q = \frac{Q_B}{q} = \sqrt{\frac{2K_s \epsilon_0 \phi N_D}{q}}$$

$$\phi = E_g \quad \text{for weak inversion} \quad (4.9)$$

$$\phi = E_g + 6kT \quad \text{for strong inversion.}$$

Q_B is the bulk charge and N_D is the dopant concentration.

Using $\frac{1}{2}E_g$ as the flat band surface potential, the n^+ region reaches weak and strong inversion at surface state densities of $5.2 \times 10^{12} \text{ cm}^{-2}$ and $6 \times 10^{12} \text{ cm}^{-2}$ respectively. This calculation only accounts for matching charges in the depleted MCT boundary and does not include other charge losses due to recombination in the insulating layer.

Prior to adding any models for tunneling, we conducted PISCES simulations using enough fixed charge to invert the surface. Without including tunneling, the simple band bending model does not account for increased currents in irradiated diodes.

Keldysh and Kane were the first to develop direct (BTB) tunneling models based on quantum mechanical processes in semiconducting materials. Their models include direct tunneling of electrons and holes through a triangular barrier across a semiconductor junction. Figure 4.6 shows the band configuration and potential barrier presented to an electron in the p side valence band. In this figure, tunneling is possible when the electron has sufficient energy to pass through the barrier presented and still have energy greater than the conduction band on the n side.

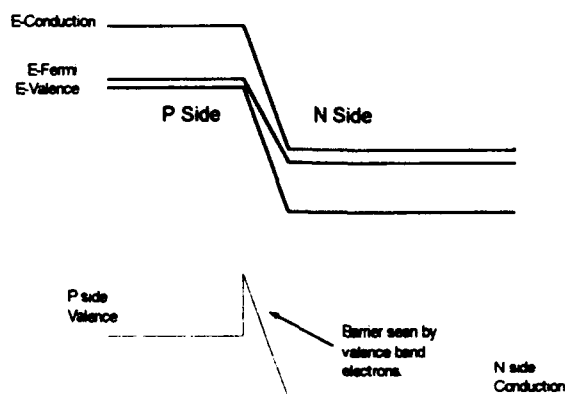


Figure 4.6. Reverse bias band diagram with the potential barrier.

The simplified version of the model is given by:

$$R_{\text{BTB}} = -B|\xi|^\sigma D(\xi, \psi, E_{\text{fn}}, E_{\text{fp}}) e^{-\frac{\xi_0}{|\xi|}} \quad (4.10)$$

In equation 4.10, experiment shows that $\sigma = 2$ for direct transition semiconductors. ξ is the local electric field, ψ the electrostatic potential, and E_{fn} and E_{fp} the n and p quasi fermi levels respectively. ξ_0 is a constant which accounts for a sufficient electric field for motivating the electron or hole across the tunneling junction. The prefactor B is a temperature independent constant that accounts for several constants used in the formula, to include \hbar and the electron effective mass.

The function D accounts for the relative energy level of valence band electrons in the p side to that of the conduction band on the n side. This function becomes one, when the band energies present a probable tunneling condition. The original form of this equation found by Kane and Keldysh was not in a closed form and thus not usable in a numerical simulator. Hurkx et al developed an expression for use in a simulator by eliminating the electric field dependence and solving it using the Poisson equation to eliminate the electric field. Their model for D is:

$$D(\psi, E_{\text{fn}}, E_{\text{fp}}) = \frac{1}{1 + e^{\frac{(-E_{\text{fp}} - q\psi)}{kT}}} - \frac{1}{1 + e^{\frac{(-E_{\text{fn}} - q\psi)}{kT}}} \quad (4.11)$$

This function is accurate provided the electron and hole density are not near the intrinsic level, which occurs within the junction. When this occurs the function approaches 0.5 instead of one. Hurkx recommends making $D=1$ at all mesh points where the hole or electron current density is a fraction (e.g., 10^{-3}) of $qn_e v_s$, where v_s is the saturated drift velocity. However, this method causes PISCES to become unstable with small band gap materials, due to the abrupt change in D (and thus R_{BTB} , n and p) at a junction. We assumed a different approach to this solution based on the requirement for a smooth transition from the no tunneling to the tunneling process, and the physical characteristics of MCT.

Equation 4.11 multiplied by the exponential term in equation 4.10⁴, plotted as a function of electric field and using the suggestions of Hurkx, reveals it to be nearly a step function. We replaced this very abrupt function by a Boltzman function which transitions

⁴ ξ_0 is an arbitrary constant, unknown for MCT. It is later defined through the effective electric field function.

smoothly from zero to one when tunneling is probable. The Boltzmann form as a function of electric field (ξ) used is:

$$F_{\text{Boltz}}(\xi) = \frac{A_1 - A_2}{1 + e^{\frac{\xi - x_0}{dx}}} + A_2. \quad (4.12)$$

A_1 and A_2 determine the start and finish levels and are zero and one respectively. The term x_0 determines the point where the function reaches the half way point between A_1 and A_2 . The dx term establishes the spread in the overall transition region. Figure 4.7 shows the Boltzman function plotted with $D \times \exp(-F_0/|F|)$.

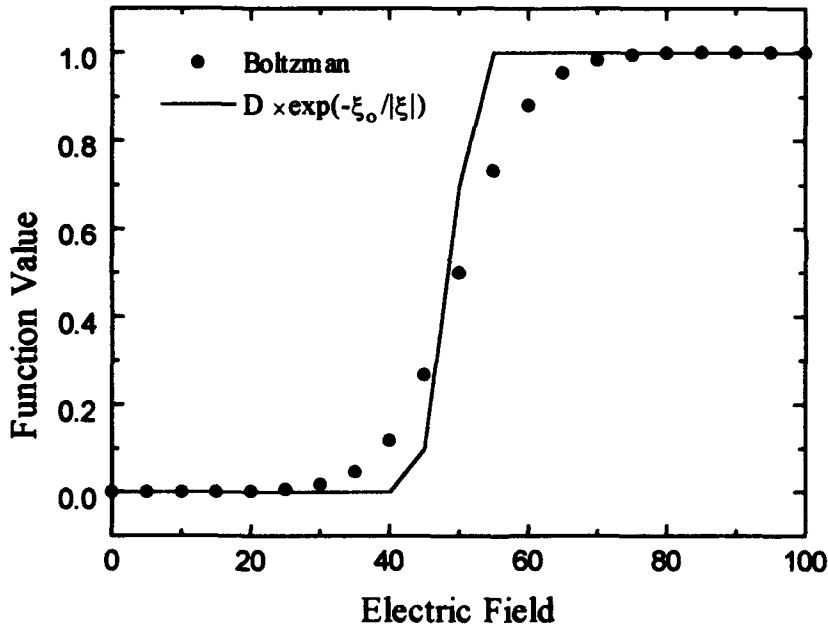


Figure 4.7. A Boltzman function fit to data.

To determine the electric field required to cause a transition from zero to one, we used the triangular barrier potential barrier and solved for a quantum mechanical transfer of the electron through the barrier. This can be done using the Shrodinger equation and solving for both the transfer and reflected coefficients. The x_0 term was set equal to the point where the transmission probability was equal to 0.5. The final equation for the BTB tunneling is

$$R_{\text{BTB}} = -B|\xi|^{\sigma} F_{\text{Boltz}}(A_1, A_2, x_0, dx, \xi) \quad (4.13)$$

where; B is $30 \text{ cm}^{-1} \text{ V}^{-2} \text{ s}^{-1}$, $\sigma=2$, $x_0=683 \text{ V/cm}$ and $dx=60$.

Equation 4.13 was added to PISCES as a recombination term in the same way SRH and Auger. It was then tested by comparing the I-V curves from strongly reverse biased P-N diodes, where band to band tunneling becomes dominant. This was done to validate the results of the model prior to attempting the radiation effects modeling. Figure 4.8 gives the results of the modified PISCES with and without the tunneling models.

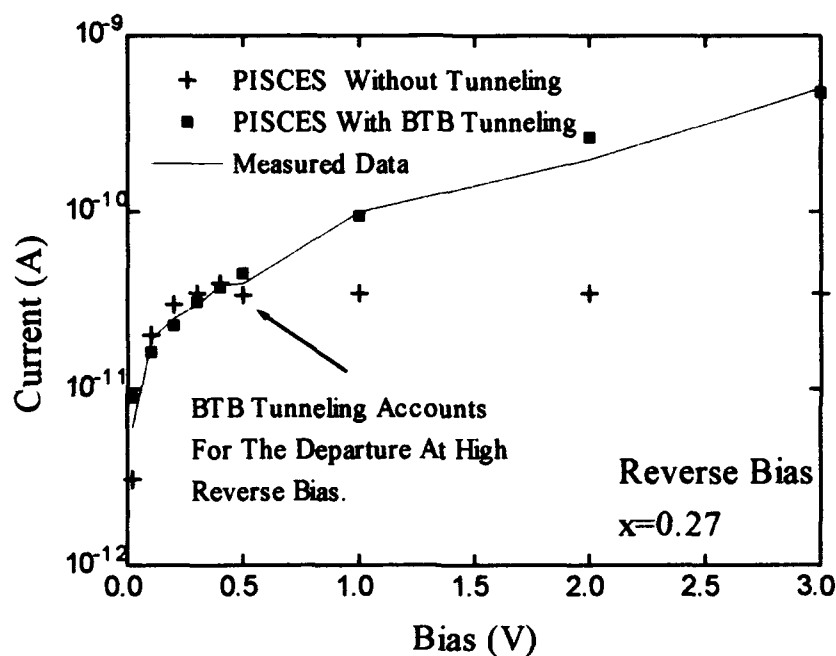


Figure 4.8. Reverse bias simulation of a P-N junction with and without the tunneling models.

To see the effect of the band to band tunneling model in irradiated diodes, we placed 10^{12} cm^{-2} negative fixed charges along the MCT/passivant boundary in a simulated diode. We then compared the I-V results to those from an OMVPE diode irradiated to 625 krad(Si) by a ^{60}Co source. Negative fixed charge is used based on literature information on MCT MIS devices. The results in 4.9 show a reasonable agreement at reverse bias voltages less than 0.4 V. This voltage regions also indicates a maximum current is being reached as indicated by the 250 and 625 krad following the same trace. The physical basis for this maximum comes from the material becoming fully depleted at the surface. Increased the surface charge doesn't bend the bands further, but simply moves the depletion region further into the bulk, which doesn't contribute to increased current. The

band to band model also reaches this maximum even when the fixed charge is increased by 2 orders of magnitude. The correlation between these maximums is an indicator of the validity of the BTB tunneling process in the irradiated diodes.

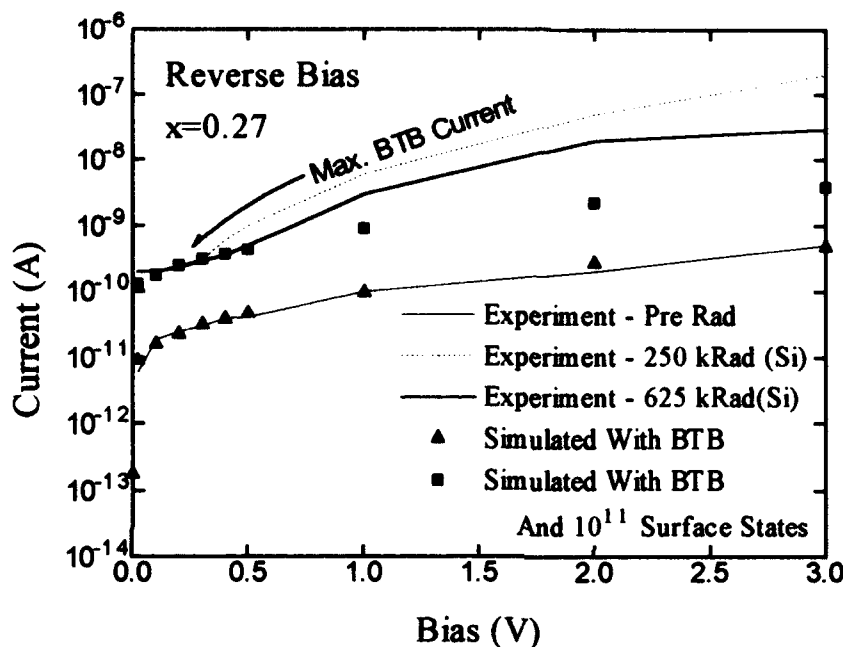


Figure 4.9. Results of simulated radiation effects compared to measured data from irradiated diodes.

At a reverse bias above 0.4 V there is a departure from the measured and simulated currents. The slope of the curve follows an electric field squared dependence, which is indicative of junction tunneling. Based on this we suspect that this is TAT which is was not yet modeled.

Developing the models for TAT are much more involved. Since we assume that the OMVPE devices are relatively pure, data from irradiated diodes must be used to formulate models for TAT. TAT can be modeled using several approaches, most often by the principle of detail balance. This method requires knowledge of the trap levels associated with the tunneling, and then predicting the probability of transfer based on their relative energy levels. However, the trap formation in MCT is not well known, and can be different for n and p type materials. The induced trap energy levels must be obtained separately for both regions. This can be done using the results of total dose irradiation on n and p type samples and DLTS studies.

SECTION 5

CONCLUSIONS

Most significant to the MCT modeling of radiation effects is that the MCT production line is operating and we have students producing quality devices. We have begun to explore devices that respond in a higher wavelength region and the results are quite promising for the OMVPE growth method. Additionally, we have begun to explore extrinsic doping methods and device design using OMVPE growth, and expect to begin production of these devices in late spring or early summer 1993.

We made much progress in our modeling, especially in the area of tunneling in MCT. Using the fundamental results of the tunneling process we modified models found in the literature to depict the physical nature of BTB tunneling and can show that it accounts for current processes in unirradiated diodes. We based these modifications on physical requirements of PISCES and the stability of the solution. In the same way, we can show BTB tunneling accounts for current increases in irradiated P-N diodes, when we assume radiation induced trapped negative charge at the MCT and passivant layer.

To complete the modeling efforts, we must obtain more data regarding radiation effect on our diodes. We plan to conduct a series of tests to explore trap formation, carrier concentration, and current enhancement effects due to irradiation. Most important to these experiments is that all irradiation and characterization will be done at low temperatures to reduce thermal annealing effects. We have begun research in building an advanced low temperature irradiation and characterization chamber for this purpose.

Further studies must include expanding our efforts beyond our initial diode structures. This can be done once we account for all of the post irradiation leakage processes in our structures. This is a focus of our planned experiments. Most important, the studies must include manufacturing techniques that are most prominent in current production line technology, such as LPE growth and ion implantation. Pre- and post irradiation characteristics must be compared to our models to establish their validity for irradiation simulations. Since we do not do these processes at RPI, we must coordinate for well-characterized samples from vendors or manufacturers.

SECTION 6

REFERENCES

- Brice, J., and Capper, P. Properties of Mercury Cadmium Telluride. INSPEC, London and New York, 1987.
- DeWames, R.; Bajaj, J.; Yao, E. S.; and Williams G. M. "Laser Induced Effects in HgCdTe Photovoltaic Devices." *Journal of Vacuum Science and Technology*, A7(2), (January 1989): 536-42.
- Ghandi, S. K. Theory and Practice of Microelectronics. John Wiley, New York, 1977.
- Kane, Evan O. "Theory of Tunneling." *Journal of Applied Physics*, vol. 32, (1961): 83-86.
- Madarasz, F. L.; Szmulowicz, F.; and McBath, J. R. "Intrinsic Carrier Concentrations and Effective Masses in $\text{Hg}_{1-x}\text{Cd}_x\text{Te}$." *Journal of Applied Physics*, 58, (1985), 361-65.
- Mallon, C. E.; Naber, J. A.; Colwell, J. F.; and Green, A. B. "Effects of Electron Radiation on the Electrical and Optical Properties of HgCdTe." *IEEE Transactions in Nuclear Science*, 20, (1973): 214-23.
- Moriwaki, M. M.; Srour, J. R.; and Lou, L. F. "Ionizing Radiation Effects on HgCdTe MIS Devices." A Paper Submitted for Publication in *Transactions in Nuclear Science*.
- Morral, D. G. "Electron Irradiation in p-Type Mercury Cadmium Telluride." Master Thesis, Naval Post Graduate School, Monterey, California, 1985.
- Parat, K. K. "Studies On $\text{Hg}_{1-x}\text{Cd}_x\text{Te}$ Grown by OMVPE (DAG): Material Characterization and Devices." Ph.D. dissertation, Rensselaer Polytechnic Institute, Troy, New York, 1991.
- Parat, K. K.; Taskar, N. R.; Ehsani, H.; Bhat I. B.; and Ghandhi, S. K. "Selective Annealing for the Planar Processing of HgCdTe Devices." *Journal of Vacuum Sciences and Technology*, B9(3), (1991), 1625-31.
- Petrosky, James C. "Characterization of $\text{Hg}_{1-x}\text{Cd}_x\text{Te}$ Diodes Using PISCES-IIB and Implications to Radiation Effects." Master's Thesis, Rensselaer Polytechnic Institute, Troy, New York, 1992
- Pinto, M. R.; Rafferty, C. S.; and Dutton R. W. PISCES II: Poisson and Continuity Equation Solver. Stanford Electronics Library, 1984.

- Sarusi, G., Eger, D., and Zemel, A. "Degradation Mechanisms of Gamma Irradiated LWIR HgCdTe Photovoltaic Detectors." A Report Based on a Portion of a Dissertation for Requirements for the Ph.D. in Tel Aviv University.
- Schmit, J. L. "Intrinsic Carrier Concentration of $\text{Hg}_{1-x}\text{Cd}_x\text{Te}$ As a Function of x and T Using $k \cdot p$ Calculations." *Journal of Applied Physics*, 41(7), (1970): 2876-82.
- Srour, J. R.. "Displacement Damage Effects in Electronic Materials, Devices, and Integrated Circuits." From Tutorial Short Course Notes Presented at the 1988 IEEE Nuclear and Space Radiation Effects Conference, Portland, Oregon, 1988.
- Sze, S. M. Physics of Semiconductor Devices. 2d Edition, Wiley, New York, 1981.
- Taskar, N. "Growth and Characterization of Extrinsic n and p-type Doped $\text{Hg}_{1-x}\text{Cd}_x\text{Te}$." Ph.D. dissertation, Rensselaer Polytechnic Institute, New York, 1990.

APPENDIX A

SUBMITTED PAPERS

This appendix contains papers submitted for conferences and journals during the course of this research.

**AN INNOVATIVE APPROACH TO MODELING CURRENT
ENHANCEMENT EFFECTS DUE TO TOTAL DOSE
IONIZING RADIATION IN $\text{Hg}_{1-x}\text{Cd}_x\text{Te}$ PHOTODIODES. ¹**

J. C. Petrosky, J. W. Howard, and R.C. Block
Gaertner LINAC Laboratory
Rensselaer Polytechnic Institute, Troy, NY 12180

I. Bhat
Electrical, Computer, and Systems Engineering
Rensselaer Polytechnic Institute, Troy, NY 12180

M. C. Stauber
Grumman Corporate Research Center, Bethpage, NY 11714

¹Portions of this work were funded by the Defense Nuclear Agency

AN INNOVATIVE APPROACH TO MODELING CURRENT ENHANCEMENT EFFECTS DUE TO TOTAL DOSE IONIZING RADIATION IN $\text{Hg}_{1-x}\text{Cd}_x\text{Te}$ PHOTODIODES.

J. C. Petrosky, J. W. Howard, and R.C. Block
Gaertner LINAC Laboratory, Rensselaer Polytechnic Institute, Troy, NY 12180

I. Bhat
Electrical, Computer, and Systems Engineering, Rensselaer Polytechnic Institute, Troy, NY 12180

M. C. Stauber
Grumman Corporate Research Center, Bethpage, NY 11714

ABSTRACT

A new approach to modeling increased tunneling current in irradiated $\text{Hg}_{1-x}\text{Cd}_x\text{Te}$ photodiodes is demonstrated, by first simulating unirradiated ones. Results from irradiation aid in developing models required for simulating enhanced tunneling currents.

Introduction

$\text{Hg}_{1-x}\text{Cd}_x\text{Te}$ (MCT) photodiodes are typically used as infrared detectors in various space applications. Ionizing radiation can degrade their performance by increasing trapped charge in the passivating layers surrounding the pn junction. This ultimately results in increased tunneling currents across the junction. Since the passivating layer is required for device operation, this problem must be addressed in order to completely model device behavior before and after irradiation. The major difficulty with modeling this behavior is that until recently, MCT diodes could not be produced pure enough to separate the junction and tunneling currents. Because of this, simple device characterization becomes very complicated. This leads to difficulty in establishing the proper device characteristics, prior to adding the complications induced by the radiation damage.

Approach

Our approach begins with the growth and modeling of relatively pure devices. These steps are absolutely necessary to ensure that device simulation accurately portrays the intrinsic electrical characteristics of the device. Once this is accomplished, we add models for radiation induced

tunneling with reasonable assurance that the electrical characterization is accurately modeled. Until recently, devices of sufficient purity were not able to be grown. However, advancements in organometallic vapor phase epitaxy (OMVPE) technology and selective annealing have resulted in MCT devices with I-V relationships which approach ideal limits. Since this device manufacturing method is being explored at Rensselaer Polytechnic Institute (RPI), device characterization and design parameters are well known for irradiation and modeling purposes.

This is the first time that MCT diode simulations have been accessible for exploring radiation effects in MCT.

MCT Growth and Device Characteristics

RPI was the first and only university group to undertake research in OMVPE for the growth of MCT. This method is unique in that the CdTe layer is deposited immediately after MCT growth in the same reactor so that it does not get exposed to air. It was responsible for producing MCT diodes of the lowest leakage currents reported. Hall effect and photoluminescent studies verify the assumption that these devices are relatively defect free. We believe this in-situ grown CdTe is better than ZnS for passivating MCT diodes because of their similar lattice structure. In addition, CdTe is more stable than ZnS under radiation. MCT characteristics for this growth method have been reported in the literature [1-4].

In addition to the OMVPE growth and CdTe

passivation, the diodes selected for our study were fabricated in a unique way to inhibit any irregular device characteristics. The as-grown layers are p-type with carrier concentrations of 10^{17} cm^{-3} . PN junctions are formed by selectively annealing Hg into exposed portions of the wafer, heated by RF heating elements. This causes a type change due to diffusion of Hg into the MCT, with carrier concentrations of 10^{15} cm^{-3} . The low carrier concentration reduces the overall differential in concentration across the junction, and reduces band to band tunneling. Selective annealing avoids placing damage in the device, which would be unavoidable with ion implantation. This effectively reduces trap assisted tunneling across the junction.

Simulation of Unirradiated Diodes

Initial I-V simulations of MCT diodes using PISCES[5] gave up to a three order of magnitude difference between the measurements and simulations. Forward bias results are shown in Figure #1. The results of the reverse bias were also inaccurate.

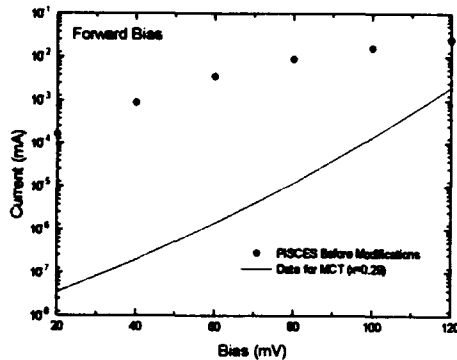


Figure 1: Initial PISCES simulations results compared to measurements

An initial investigation revealed that several PISCES models required modification to produce parameters necessary for MCT simulation. We modified PISCES by adding models for MCT energy gap, intrinsic concentration, and band density of states. These are needed since they deviate greatly from the PISCES parameter calculations and demonstrate a strong dependence on the composition (x) and temperature (T). They are applicable to $0.2 < x < 0.4$ and $70 < T < 150 \text{ K}$, and bias of $-60 < V < 120$

mV. In this region tunneling currents across the pn junction are negligible. We also included 17 material parameters which are constant over the required range. The forward and reverse bias results are shown in Figures 2 and 3 which show excellent agreement between simulated and measured results.

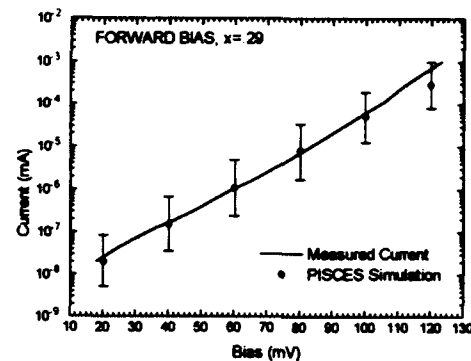


Figure 2: Reverse Bias Diode Simulation.

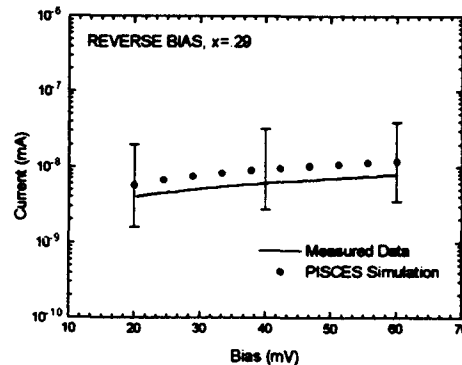


Figure 3: Reverse Bias Diode Simulations.

Modeling Radiation Effects

The next part of our modeling focuses on developing models for the tunneling associated with the passivation trapped charge induced band bending. Tunneling falls into two categories, band-to-band (BTB) and trap assisted tunneling (TAT).

BTB is associated with sharply bent bands in the material. This occurs in both unirradiated and irradiated MCT devices. In the unirradiated diodes, the bands are sharply bent due to heavy doping or a strong reverse bias. Once irradiated, sharp band

bending also occurs along the passivation boundary, due to trapped charges in the passivation layer. BTB tunneling can be investigated using either situation.

We developed BTB tunneling models for the OMVPE growth diodes using the theory developed by Keldysh and Kane [6], and approximated the D function as a boltzman function equal to 0.5 when valence band electrons have a 50% probability of tunneling to the conduction band. After inserting this model into PISCES we compared simulations to reverse bias characteristics of the OMVPE diodes at higher reverse bias. The results in Figure 4 show the agreement of our model to the tunneling region in the diode at high reverse bias.

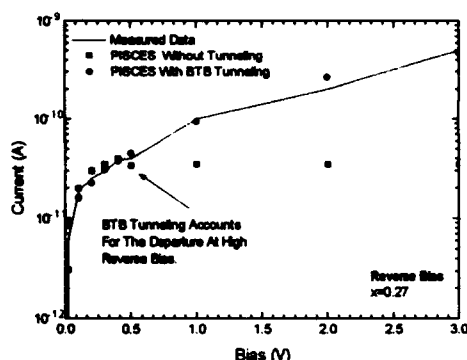


Figure 4: Simulations Using the BTB Tunneling Model

To see the effect of the band to band tunneling model in irradiated diodes, we placed 10^{12} cm^{-2} negative fixed charges along the MCT/passivant boundary in a simulated diode. We then compared the I-V results to those from an OMVPE diode irradiated to 625 krad(Si) by a ^{60}Co source. Negative fixed charge is used based on literature information on MCT MIS devices [7]. The results in Figure 5 show a reasonable agreement at reverse bias voltages less than 0.4 V. At this bias, a threshold is met as indicated by both 250 and 625 krad curves. The band to band model also provides this threshold even when the fixed charge is varied by 2 orders of magnitude. This threshold is due to the maximum band bending and thus maximized tunneling generation current near the surface. The correlation between the threshold regions is a clear indicator of the validity of the BTB tunneling process in the

irradiated diodes.

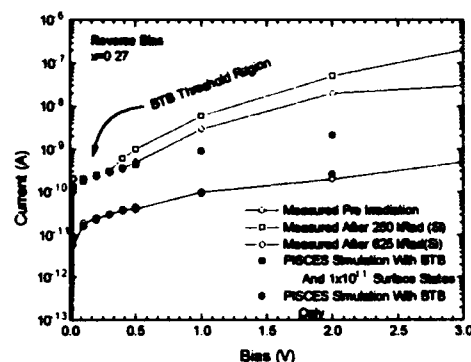


Figure 5: Post Irradiation Simulations.

At a reverse bias above 0.4 V there is a departure from the measured and simulated currents. The slope of the curve follows an electric field squared dependence, which is indicative of junction tunneling. Based on this we suspect that this is TAT which is was not modeled.

Developing the models for TAT are much more involved. Since we assume that the OMVPE devices are relatively pure, data from irradiated diodes must be used to formulate models for TAT. TAT can be modeled using several approaches, most often by the principle of detail balance [8]. This method requires knowledge of the trap levels associated with the tunneling, and then predicting the probability of transfer based on their relative energy levels. However, the trap formation in MCT is not well known, and can be different for n and p type materials [9]. The induced trap energy levels must be obtained separately for both regions. This can be done using the results of total dose irradiation on n and p type samples and DLTS.

Conclusions

We have shown that by modeling relatively pure devices, MCT pn junction electrical characteristics can be simulated using a numerical device simulator. Using this basis, theoretical phenomenon can be modeled and applied, to validate theories. We

included BTB tunneling which is assumed to contribute to excess leakage in irradiated photodiodes. This accounts for the departure from the ideal characteristics found in the higher reverse bias of inirradiated diodes, and the threshold reached at the low reverse bias of irradiated diodes. Modeling efforts based on radiation induced trap formation can lead to models for TAT which can be applied and tested to account for the overall leakage.

Devices", Ph.D. Thesis, Rensselaer Polytechnic Institute, Troy, New York, 1991.

REFERENCES

- [1] S.K.Ghandhi, K.K.Parat, H.Ehsani and I.B.Bhat, "High Quality Planar HgCdTe Photodiodes Fabricated by Organometallic Epitaxy", Appl. Phys. Lett. 58, 828,(1991).
- [2] N.R.Taskar, I.B.Bhat, K.K.Parat, S.K.Ghandhi and G.J.Scilla, "Extrinsic P Doped HgCdTe Grown by Direct Alloy Growth Organometallic Epitaxy", J.Vac. Sci. Tech. B9, 1705(1991).
- [3] S.K.Ghandhi, N.R.Taskar, K.K.Parat and I.B.Bhat, "Indium Doping of N-type HgCdTe Layers Grown by Organometallic Vapor Phase Epitaxy", Appl. Phys. Letters, 57(3), 252(1990).
- [4] K.K.Parat, H.Ehsani, I.B.Bhat and S.K.Ghandhi, "Selective Annealing For the Planar Processing of HgCdTe Devices", J.Vac Sci Tech. B9, 1625(1991).
- [5] M.R. Pinto, C. S. Rafery, and R. W. Dutton. PISCES II: Poisson and Continuity Equation Solver, Stanford Electronics Library, 1984.
- [6] Evan O. Kane. "Theory of Tunneling", Journal of Applied Physics, Volume 37, Number 1, 1961.
- [7] R. DeWames, J. Bajaj, E.S. Yao, and G. M. Williams. "Laser Induced Effects in HgCdTe Photovoltaic Devices", Journal of Vacuum Science and Technology, A7(2), 536, 1989.
- [8] S. K. Ghandi, Theory and Practice of Microelectronics, John Wiley, New York, 1977.
- [9] K. K. Parat, "Studies On HgCdTe Grown by OMVPE (DAG): Material Characterization and

AN INNOVATIVE APPROACH TO SIMULATING TOTAL DOSE IONIZING RADIATION ENHANCED TUNNELING IN $Hg_{1-x}Cd_xTe$ PHOTODIODES.

J. C. Petrosky, J. W. Howard, I. Bhat and R.C. Block
Rensselaer Polytechnic Institute, Troy, NY 12180

M. C. Stauber

Grumman Corporate Research Center, Bethpage, NY 11714

ABSTRACT

A new approach to modeling increased tunneling currents in irradiated $Hg_{1-x}Cd_xTe$ photodiodes is demonstrated, by first simulating unirradiated ones. Results from irradiation aid in developing models required for simulating enhanced tunneling currents.

Introduction

$Hg_{1-x}Cd_xTe$ (MCT) photodiodes are used as infrared detectors in space applications. Ionizing radiation degrades performance by increasing trapped charge in passivating layers surrounding the pn junction. This results in increased tunneling currents.

Approach

Our approach begins with the growth and modeling of relatively pure devices by OMVPE and selective annealing. This is absolutely necessary to ensure that device simulation accurately portrays the intrinsic electrical characteristics of the device. Since this device manufacturing method is being explored at RPI, device characterization and design parameters are well known for irradiation and modeling purposes.

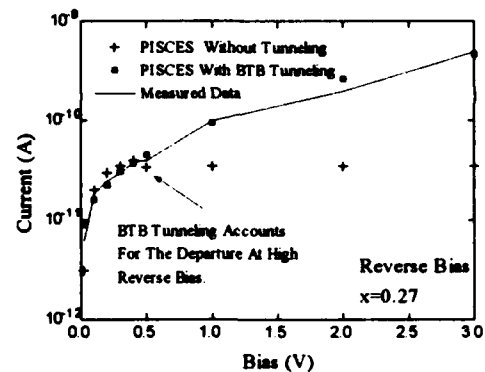
Simulation of Unirradiated Diodes

Initial I-V simulations of MCT diodes using PISCES gave up to a three order of magnitude difference between measurements and simulations. PISCES required modifications to produce parameters necessary for MCT simulation. We modified PISCES by adding models for MCT energy gap, intrinsic concentration, and band density of states. These are needed since they deviate greatly from the PISCES parameter calculations and demonstrate a strong dependence on the composition (x) and temperature (T). We also included 17 material parameters which are constant over the required range. This produced I-V results which accurately portrayed those of the OMVPE grown MCT diodes.

Modeling Radiation Effects

The next part of our modeling focused on

developing models for the tunneling associated with the passivation trapped charge induced band bending. We developed direct tunneling models using the theory developed by Keldysh and Kane and approximated the D function as an appropriate Boltzman function. After inserting this model into PISCES we compared simulations to diode reverse bias characteristics at high reverse bias. The results in the figure below show the agreement of our model to the tunneling region in the diode where direct tunneling is present in unirradiated diodes.



To see the effect of the band to band tunneling model in irradiated diodes, we placed 10^{12} cm^{-2} negative fixed charges along the MCT/passivant boundary in a simulated diode. We then compared the I-V results to those from an OMVPE diode irradiated to 625 krad(Si) by a ^{60}Co source. The results show a reasonable agreement at reverse bias voltage less than 0.4 V.

Conclusions

We have shown that by modeling relatively pure devices, MCT pn junction electrical characteristics can be simulated using a numerical device simulator. We included BTB tunneling which is assumed to contribute to excess leakage in irradiated photodiodes. This method can also be extended to modeling trap assisted tunneling using results of radiation studies, and DLTS analysis.

APPENDIX B

RADIATION TEST PLAN

This appendix contains the radiation test plan used to gain additional data for this research.

Test Plan
Hg_{1-x}Cd_xTe (MCT) Total Dose Response

James C. Petrosky
Rensselaer Polytechnic Institute
Troy, New York 12180-3590
(518) 276-6650

February 8, 1993

1. Introduction

This document describes the tests to be done at the LINAC facility at RPI. It establishes requirements for the tests before their commencement. This document does not negate coordination and exchange of information between coordinators, supervisors and technicians, but opens the dialogue between them regarding use of the LINAC facility.

2. Test Objectives

Our objective is to explore the effects of total dose ionizing radiation on the electrical characteristics of passivated MCT layers and pn diodes at low temperatures (77K). These diodes/layers were fabricated at RPI as part of our research in MCT growth and radiation effects. We will use the information obtained from these tests to evaluate the total dose hardness of the devices grown by OMVPE and as a guide in developing models in a device simulator. The parameters of interest and test procedures are given in the table.

| PARAMETERS OF INTEREST AND TEST PROCEDURES | |
|--|------------------|
| MCT X=.23 | |
| T=77°K | |
| Growth Method: OMVPE, doped by annealing. | |
| PARAMETER | TEST PROCEDURE |
| Doping Level N_d , N_a | Hall Effect |
| Mobility μ_n , μ_p | Hall Effect |
| I-V (-4V→200mV) | I-V curve tracer |

We will study these parameters as a function of total dose using three MCT sample types: pn mosaic structures, n wafer passivated with ZnS, and p type wafer with CdTe. A detailed analysis of the devices and test procedures is given in section 5.

3. Proposed Schedule

Given the busy LINAC schedule and our desire to do the tests at the earliest opportunity, we will remain flexible in scheduling LINAC time. At the approval of the facility director, we will attempt to fit in our experiments after other patrons finish if time is available.

We based the following testing times on recent experiences at Grumman corporation and made allowances for the facility layout. Tests are described in section 5, "Description of Tests."

Dosimetry: Analysis of dosimetry in two dewar/liquid nitrogen systems.

TIME Estimate: One hour for setup, irradiation and TLD reading/analysis.

I-V Irradiation: Irradiate pn diodes and take I-V measurements.

TIME Estimate: Four hours for each diode, including set up, measuring and occasional refilling of liquid nitrogen.

Bulk Sample Irradiation: Irradiate bulk samples and conduct Hall effect measurements.

TIME Estimate: Four hours for each sample, including set up, measuring and occasionally refill the liquid nitrogen.

4. Test Priority

The tests listed in section one will provide much needed data for our research program. However, if time or equipment is not permissive for this testing, we will place priority on the bulk layer tests, leaving the pn diodes for a later date.

5. Description of Tests

Our goal is to find the effect of total dose ionizing radiation on the electrical characteristics of passivated MCT at operating temperature (77K) while minimizing thermal annealing. **It is therefore imperative that we don't change the conditions during our measurements by raising the temperature above 100K (the trapped carrier freeze in).** To accomplish this, the irradiations and analysis must be done inside dewars filled with liquid nitrogen.

All irradiation will be done with a Bremsstrahlung target to produce gamma irradiation. The beam power should be set at its optimal range (17MeV), and dosimetry obtained by locating the tests devices at the appropriate distance from the output window. The maximum dose rate for this test is 0.66 kRad/sec (2.5 MRad/hr).

The tests are divided into two types; bulk and diode tests. The beam size at our dose rate should be sufficient to irradiate both types simultaneously.

5.1. Bulk Layer Tests

Bulk layer tests will be done on n and p type MCT samples. We will progressively irradiate and conduct Hall effect measurements on each of them. Samples will be mounted on a test probe before the start of the tests, and then placed in a Hall effect dewar. The test fixture is shown in Figure #1. The test procedure for both n and p type is the same.

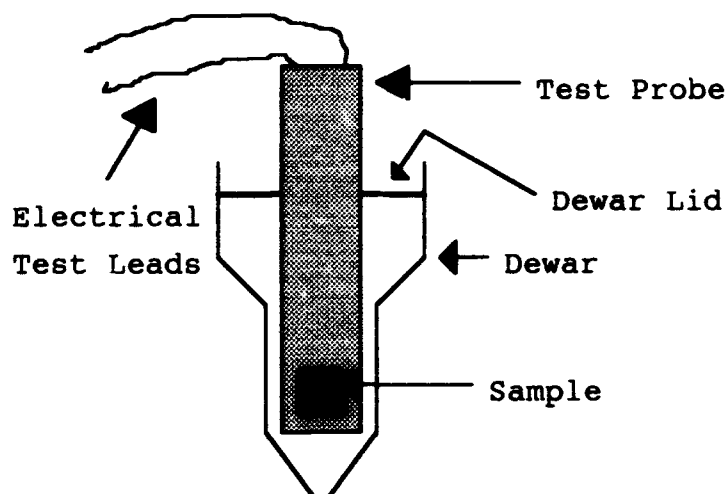


Figure 1: Hall Effect dewar system.

Tests will be performed in the following manner, after dosimetry is complete.

| <u>Step</u> | <u>Procedure</u> |
|-------------------------|---|
| 1 | Cool devices in liquid nitrogen dewar until we are assured of temperature uniformity (approximately 10 minutes). |
| Characterization | |
| 2 | Conduct Hall effect measurements on sample. |
| 3 | Place in electron beam and irradiate to 200 krad(Si) additional dose at 0.66 kRad/sec. |
| 4 | Repeat steps 2 through 3 until a total dose of 2 Mrad(Si) is reached, then conduct step 2 for a final analysis. If the p type layer does not invert to n type by this total dose, continue with the above procedures on the p type layer. Increase the dose in step 3 to 0.5 Mrad(Si) until we reach 10 Mrad. |

5.2. pn Diode Tests

The pn diodes are made by OMVPE and selective annealing. P-type contacts are gold, and n-type connections are indium. A diagram of these is shown in Figure 2. The device is mounted on a gold plated alloy mounting bracket for stability and can be positioned in the dewar using a styrofoam mount.

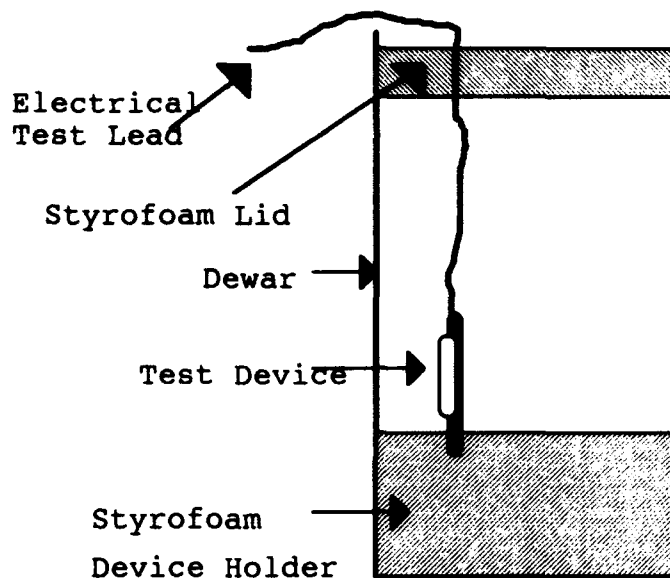


Figure 2: I-V Irradiation System.

The Keithley source measurement unit will be used to trace the I-V characteristics of the diodes from -3 to 0.2 V. Current must be measured in the 10pA range, which requires special handling to reduce noise. Two procedures will help in accomplishing our measurements at this level. We must remove the devices from areas with high noise sources, such as the beam and control rooms. The best location that is accessible during the tests is the small stock room located behind the LINAC control room. We must test this area before conducting the tests. Additionally, we can build an EM Faraday box and use the Keithley remote source option. We are currently pursuing building such a box.

The tests will be done in the following manner, after dosimetry is complete.

Step Procedure

- 1 Cool devices in liquid nitrogen dewar until we are assured of temperature uniformity (approximately 10 minutes).

IV Measurements

- 2 Conduct IV curve measurements from -4V to 240mV. The measurement should be done twice by reversing the voltage sequence. This must be done for each device.
- 3 Ground leads and place in electron beam. Irradiate for 200 krad(Si) additional dose at one kRad/sec.
- 4 Repeat steps 2 and 3 until a total dose of 2 Mrad(Si).

5.3. Responsibilities.

5.3.1. Petrosky

- Update test plan.
- Prepare and mount wafers and diodes in the test devices.
- Provide equipment for measuring I-V relationships and hall effect for bulk samples.
- Conduct measurements during the experiments.

5.3.2. LINAC Facility

- Have sufficient liquid nitrogen on-hand for the experiments.
- Provide technical assistance for dosimetry.
- Prepare LINAC with a Bremsstrahlung target before experiments.

6. Special Requirements

6.1. Radiation Safety

Safety in the test area is very important. All safety procedures established by the RPI LINAC facility will be followed. Keithley test equipment will be connected so all leads will be covered or connected. These leads can reach lethal currents during operations.

6.2. Data Analysis

Data analysis is simplified by using the computer programs designed for the Keithley and the Hall effect measurement equipment. Besides information requested by these programs, we must record the initial dosimetry information, incremental and total dose for each run.

7. Point of Contact

Please address any questions or suggestions to:

James C. Petrosky

HOME: (518) 786-1328

EMAIL: petrosky@sunhoward.ne.rpi.edu

DISTRIBUTION LIST

DNA-TR-93-50

DEPARTMENT OF DEFENSE

ADVANCED RESEARCH PROJECT AGENCY
ATTN: ASST DIR ELECTRONIC SCIENCES DIV
ATTN: R REYNOLDS

ASSISTANT TO THE SECRETARY OF DEFENSE
ATTN: EXECUTIVE ASSISTANT

DEFENSE ELECTRONIC SUPPLY CENTER
ATTN: DESC-E

DEFENSE INTELLIGENCE AGENCY
ATTN: DIW-4
ATTN: DT-1B

DEFENSE NUCLEAR AGENCY
ATTN: RAEE TREE
2 CY ATTN: TITL

DEFENSE SYSTEMS SUPPORT ORGANIZATION
ATTN: JNGO

DEFENSE TECHNICAL INFORMATION CENTER
2 CY ATTN: DTIC/OC

DNA PACOM LIAISON OFFICE
ATTN: DNALO

FIELD COMMAND DEFENSE NUCLEAR AGENCY
ATTN: FCPF R ROBINSON

DEPARTMENT OF THE ARMY

ARMY RESEARCH LABORATORIES
ATTN: AMSRL-WT-NJ
ATTN: SLCHD-NW-TN

U S ARMY MISSILE COMMAND
ATTN: AMCPM-HA-SE-MS

U S ARMY NUCLEAR & CHEMICAL AGENCY
ATTN: MONA-NU DR D BASH

U S ARMY RESEARCH OFFICE
ATTN: R GRIFFITH

U S ARMY SPACE & STRATEGIC DEFENSE CMD
ATTN: CSSD-SL

U S ARMY STRATEGIC SPACE & DEFENSE CMD
ATTN: CSSD-SA-E
ATTN: CSSD-SD-A

U S MILITARY ACADEMY
ATTN: LTC AL COSTANTINE

USAISC
ATTN: ASOP-DO-TL BLDG 61801

DEPARTMENT OF THE NAVY

NAVAL COMMAND CONTROL & OCEAN
SURVEILLANCE CTR
ATTN: CODE 250

NAVAL POSTGRADUATE SCHOOL
ATTN: CODE 1424 LIBRARY

NAVAL RESEARCH LABORATORY
ATTN: CODE 4600 D NAGEL
ATTN: CODE 6613 A B CAMPBELL
ATTN: CODE 6813 N SAKS
ATTN: CODE 6816 H HUGHES

NAVAL SEA SYSTEMS COMMAND
ATTN: NAVSEA-081 A NEWHOUSE

NAVAL SURFACE WARFARE CENTER
ATTN: CODE H21 F WARNOCK
ATTN: CODE H23 R SMITH

NAVAL SURFACE WARFARE CENTER
ATTN: CODE H-21

NAVAL TECHNICAL INTELLIGENCE CTR
ATTN: LIBRARY

NAVAL WEAPONS SUPPORT CENTER
ATTN: CODE 6054 D PLATTETER

NAWCWPNSDIV DETACHMENT
ATTN: CLASSIFIED LIBRARY

PROGRAM EXECUTIVE OFFICE
ATTN: AIR-536T

STRATEGIC SYSTEMS PROGRAM
ATTN: JIM HOWARD SP-23

DEPARTMENT OF THE AIR FORCE

AERONAUTICAL SYSTEMS CENTER
ATTN: ASD/ENSS

AIR FORCE CTR FOR STUDIES & ANALYSIS
ATTN: AFSAA/SAI

AIR UNIVERSITY LIBRARY
ATTN: AUL-LSE

PHILLIPS LABORATORY
ATTN: PL/VTE
ATTN: F./VTEE S SAMPSON

ROME LABORATORY
ATTN: ESR

ROME LABORATORY/SUL
ATTN: RBR

WRIGHT LABORATORY
ATTN: AFWAL/ELE
ATTN: WRDC/MTE

DEPARTMENT OF ENERGY

DEPARTMENT OF ENERGY
ALBUQUERQUE OPERATIONS OFFICE
ATTN: NESD

DNA-TR-93-50 (DL CONTINUED)

LAWRENCE LIVERMORE NATIONAL LAB

ATTN: J YEE
ATTN: G POMYKAL
ATTN: W ORVIS

LOS ALAMOS NATIONAL LABORATORY

ATTN: E LEONARD

SANDIA NATIONAL LABORATORIES

ATTN: F SEXTON
ATTN: L D POSEY
ATTN: ORG 2146 T A DELLIN
ATTN: P WINKUR DIV 1332
ATTN: T F WROBEL DIV 9341
ATTN: 2140 J WOODARD

OTHER GOVERNMENT

CENTRAL INTELLIGENCE AGENCY

ATTN: OSWR/NED
ATTN: OSWR/STD/MTB

DEPARTMENT OF TRANSPORTATION

ATTN: ARD-350

NASA

ATTN: CODE 100.0 JAMES TRAINOR
ATTN: CODE 313 V DANCHENKO
ATTN: CODE 724.0 M JHABVALA
ATTN: CODE 900 E STASSINOPOULOS

NATIONAL INSTITUTE OF STANDARDS & TECH

ATTN: P ROITMAN

DEPARTMENT OF DEFENSE CONTRACTORS

ADVANCED RESEARCH & APPLICATIONS CORP

ATTN: R ARMISTEAD

AEROSPACE CORP

ATTN: A AMRAM
ATTN: C RICE
ATTN: D SCHMUNK
ATTN: G CUEVAS
ATTN: K G HOLDEN
ATTN: LEE MENDOSA
ATTN: N SRAMEK
ATTN: R KOGA

ALLIED-SIGNAL, INC

ATTN: DOCUMENT CONTROL

ANALYTIC SERVICES, INC (ANSER)

ATTN: A HERNDON
ATTN: A SHOSTAK

BDM FEDERAL INC

ATTN: D WUNSCH

BOEING CO

ATTN: D KINGSBURY
ATTN: D EGELKROUT
ATTN: ROS WOOD
ATTN: O MULKEY

BOEING TECHNICAL & MANAGEMENT SVCS, INC

ATTN: E NORMAND
ATTN: P R MEASEL
ATTN: W C BOWMAN
ATTN: W G BARTHOLET

BOOZ ALLEN & HAMILTON INC

ATTN: D VINCENT
ATTN: L ALBRIGHT

CALIFORNIA INSTITUTE OF TECHNOLOGY

ATTN: C BARNES

CHARLES STARK DRAPER LAB, INC

ATTN: J BOYLE
ATTN: N TIBBETTS

CLEMSON UNIVERSITY

ATTN: P J MCNULTY

COMPUTER PRODUCTS A DIVISION OF AMPEX

ATTN: B RICKARD
ATTN: K WRIGHT

COMPUTER SCIENCES CORP

ATTN: A SCHIFF

DAVID SARNOFF RESEARCH CENTER, INC

ATTN: R SMELTZER

E-SYSTEMS, INC

ATTN: MAIN LIBRARY

EATON CORP

ATTN: R BRYANT

ELECTRONIC INDUSTRIES ASSOCIATION

ATTN: J KINN

GENERAL ELECTRIC CO (ASD)

ATTN: D SWANT
ATTN: D TASCA
ATTN: H O'DONNELL
ATTN: J ANDREWS
ATTN: J LINNEN
ATTN: J LOMAN

GENERAL ELECTRIC CO

ATTN: B FLAHERTY
ATTN: L HAUGE

GENERAL RESEARCH CORP

ATTN: A HUNT

GEORGE WASHINGTON UNIVERSITY

ATTN: A FRIEDMAN

HARRIS CORP

ATTN: J C LEE
ATTN: J W SWONGER

HARRIS CORPORATION

ATTN: E YOST
ATTN: W ABARE

HONEYWELL INC
ATTN: R JULKOWSKI

HONEYWELL, INC
ATTN: MS 725-5

HUGHES AIRCRAFT COMPANY
ATTN: E KUBO

IBM CORP
ATTN: DEPT L75

IBM CORP
ATTN: J ZIEGLER

IBM CORP
ATTN: N HADDAD

INSTITUTE FOR DEFENSE ANALYSES
ATTN: TECH INFO SERVICES

JAYCOR
ATTN: D WALTERS

JAYCOR
ATTN: CYRUS P KNOWLES
ATTN: R SULLIVAN

JAYCOR
ATTN: L DARDA
ATTN: R POLL

JOHNS HOPKINS UNIVERSITY
ATTN: R MAURER

KAMAN SCIENCES CORP
ATTN: DASAC

KAMAN SCIENCES CORPORATION
ATTN: DASAC
ATTN: R RUTHERFORD

KEARFOTT GUIDANCE AND NAVIGATION CORP
ATTN: J D BRINKMAN

LITTON SYSTEMS INC
ATTN: F MOTTER

LOCKHEED MISSILES & SPACE CO, INC
ATTN: F JUNG
ATTN: TECHNICAL INFO CENTER

LOCKHEED MISSILES & SPACE CO, INC
ATTN: E HESSEE
ATTN: G LUM
ATTN: J CAYOT
ATTN: L ROSSI
ATTN: P BENE

LOCKHEED SANDERS, INC
ATTN: BRIAN G CARRIGG

LOGICON R & D ASSOCIATES
ATTN: D CARLSON

LORAL AERONUTRONIC
ATTN: TECHNICAL LIBRARY

LTV AEROSPACE & DEFENSE COMPANY
2 CY ATTN: LIBRARY EM-08

MARTIN MARIETTA
ATTN: J MILLER

MARTIN MARIETTA DENVER AEROSPACE
ATTN: P KASE
ATTN: RESEARCH LIBRARY

MARTIN MARIETTA TECHNOLOGIES INC
ATTN: J TANKE
ATTN: TIC/MP-30

MARTIN MARIETTA TECHNOLOGIES, INC
ATTN: H SCHISLER

MARYLAND, UNIVERSITY OF
ATTN: H C LIN

MCDONNELL DOUGLAS CORP
ATTN: R L KLOSTER

MCDONNELL DOUGLAS CORPORATION
ATTN: P ALBRECHT

MISSION RESEARCH CORP
ATTN: D ALEXANDER

MISSION RESEARCH CORP
ATTN: J LUBELL
ATTN: W WARE

MITRE CORPORATION
ATTN: J R SPURRIER
ATTN: M FITZGERALD

NATIONAL SEMICONDUCTOR CORP
ATTN: F C JONES

NORDEN SYSTEMS, INC
ATTN: N RIEDERMAN
ATTN: TECHNICAL LIBRARY

NORTHROP CORPORATION
ATTN: J R SROUR

PACIFIC-SIERRA RESEARCH CORP
ATTN: H BRODE

PHYSITRON INC
ATTN: MARK CHRISTOPHER

PHYSITRON INC
ATTN: MARION ROSE

RAND CORP
ATTN: C CRAIN

RAYTHEON CO
ATTN: D D LEE
ATTN: JOSEPH SURRO

RENSSELAER POLYTECHNIC INSTITUTE
2 CY ATTN: I BHAT
2 CY ATTN: J C PETROSKY
2 CY ATTN: J HOWARD
2 CY ATTN: R C BLOCK

DNA-TR-83-50 (DL CONTINUED)

RESEARCH TRIANGLE INSTITUTE
ATTN: M SIMONS

ROCKWELL INTERNATIONAL CORP
ATTN: V DE MARTINO

S-CUBED
ATTN: J M WILKENFELD

SCIENCE APPLICATIONS INTL CORP
ATTN: D MILLWARD
ATTN: DAVID LONG

SCIENCE APPLICATIONS INTL CORP
ATTN: J RETZLER

SCIENCE APPLICATIONS INTL CORP
ATTN: W CHADSEY

SCIENCE APPLICATIONS INTL CORP
ATTN: P ZIELIE

SCIENTIFIC RESEARCH ASSOC, INC
ATTN: H GRUBIN

SUNDSTRAND CORP
ATTN: C WHITE

SYSTRON-DONNER,
ATTN: SECURITY OFFICER

TECHNOLOGY DEVELOPMENT ASSOCIATES
ATTN: R V BENEDICT

TELEDYNE BROWN ENGINEERING
ATTN: G R EZELL
ATTN: LEWIS T SMITH

TEXAS INSTRUMENTS, INC
ATTN: J SALZMAN

TRW
ATTN: M J TAYLOR

TRW INC
ATTN: TIC

TRW SIG
ATTN: C BLASNEK
ATTN: DR D R GIBSON

TRW SPACE & DEFENSE SECTOR
ATTN: D M LAYTON

UNISYS CORPORATION-DEFENSE SYSTEMS
ATTN: P MARROFFINO

VISIDYNE, INC
ATTN: C H HUMPHREY
ATTN: W P REIDY